THE GEOLOGICAL SOCIETY OF AMERICA®

Late Miocene or older canyon incision in the northern U.S. Cordillera shown by erosion rates, incision models, and basalt flow ages

Nate Mitchell[1,†], Brian Yanites[1], Alison Duvall[2], Eugene Humphreys[3], Jonathan Perry-Houts[3], Philip Schoettle-Greene[2], and Seth Williams[2]

[1]*Department of Earth and Atmospheric Sciences, Indiana University, 1001 East 10th Street, Bloomington, Indiana 47405-1405, USA*
[2]*Department of Earth and Space Sciences, University of Washington, Johnson Hall Room-070, Box 351310, 4000 15th Avenue NE, Seattle, Washington 98195-1310, USA*
[3]*Department of Earth Sciences, University of Oregon, 100 Cascade Hall, 1272 University of Oregon, Eugene, Oregon 97403, USA*

ABSTRACT

Deep canyons along the Salmon, Snake, and Clearwater rivers in central Idaho, USA suggest long-lasting transient incision, but the timing and drivers of this incision are not well understood. The perturbation of the Yellowstone hotspot, eruption of flood basalts, and drainage of Lake Idaho all occurred within or near to this region, but the relationship among these events and incision is unclear. Here, we utilized in situ ^{10}Be cosmogenic radionuclide concentrations for 46 samples (17 new) of fluvial sediment across the region to quantify erosion rates, calibrate stream power models, and estimate incision timing. We estimate that transient incision along the Salmon River began prior to ca. 10 Ma. However, canyon age decreases to ca. 5 Ma or earlier farther to the north. For a group of tributaries underlain by basalt, we use the age of the basalt to estimate that local transient incision began between ca. 11.5 and 5 Ma. Based on these timing constraints, the canyons along the Salmon and Clearwater rivers predate the drainage of Lake Idaho. We argue that canyon incision was triggered by events related to the Yellowstone hotspot (e.g., basalt lava damming, subsidence of the Columbia Basin, reactivation of faults, and/or lower crustal flow). Furthermore, our models suggest basalt may be more erodible than the other rock types we study. We show that lithology has a significant influence on fluvial erosion and assumptions regarding river incision model parameters significantly influence results. Finally, this study highlights how geodynamic processes can exert a significant influence on landscape evolution.

INTRODUCTION

The processes shaping the Earth's surface are influenced by geodynamics, tectonics, climate, and hydrology (Willett, 1999; Kirby and Whipple, 2001; Whipple, 2004; Rowley et al., 2013; Adams et al., 2020), and landscape morphology is increasingly shown to offer a record of the interactions between these drivers (Howard, 1965; Whittaker, 2012). For example, geodynamic and tectonic processes can drive relative surface uplift, which in turn enhances landscape gravitational potential energy and fluvial erosion. Such changes in river erosion then migrate upstream through watersheds (Rosenbloom and Anderson, 1994; Niemann et al., 2001; Crosby and Whipple, 2006; Berlin and Anderson, 2007), transmitting the new base level fall rate to hillslopes (Gallen et al., 2011). Geomorphologists often target landscapes undergoing transience to learn about the nature and timing of the driving factors in a manner similar to depositional systems within the stratigraphic record (e.g., Harkins et al., 2007; Gran et al., 2013; Crow et al., 2014; Ellis et al., 2015; Schmidt et al., 2015; Pavano et al., 2016; Duvall et al., 2020; Quye-Sawyer et al., 2020; Stephenson et al., 2021). Indeed, although erosional systems involve the destruction of bedrock and removal of sediment, the geomorphic features created by erosional processes can still preserve a record of past events (Coulthard and Van De Wiel, 2012). In this study, we combine erosion rates from cosmogenic radionuclides, basalt stratigraphy, and river incision modeling of tributaries of the Salmon and Clearwater rivers in central Idaho, USA (Fig. 1) to gain insight into the recent geological history of the northern U.S. Cordillera.

Rivers in the Salmon and Clearwater watersheds flow from low-relief surfaces at high elevations to deeply incised canyons at low elevations (Fig. 1A). We therefore interpret this region to be a transient landscape, such that there is a low-erosion rate (relict) portion that preserves a previous rate of base level fall and a high-erosion rate (adjusted) portion that is eroding at the modern rate of base level fall. There are also portions of the landscape that are currently between these two endmember states. This canyon incision occurs within a wide range of lithologies (e.g., basalt, granodiorite, and gneiss; Fig. 2), and these conditions can therefore offer insight into the influence of rock properties on transient river incision and landscape evolution.

The nature and origin of landscape transience in central Idaho has been long debated, with authors over a century ago recognizing a plateau or peneplain representing an erosional surface (Lindgren, 1904; Umpleby, 1912; Blackwelder, 1912; Lindgren and Livingston, 1918). Both plateau formation and transient incision into plateaus are long-standing problems in geomorphology, with investigations into such issues frequently becoming embroiled in debates concerning the timing of and reasons for plateau formation and incision (e.g., Karlstrom et al., 2008; Flowers et al., 2008; Yang et al., 2015; Whipple et al., 2017). Potential drivers of canyon incision in central Idaho include: (1) faulting along the Salmon River suture zone (Fig. 2A; Tikoff et al., 2001; Kahn et al., 2020); (2) drainage reorganization events related to the passage of the Yellowstone hotspot, such as the drainage of ancient Lake Idaho down the proto-Snake River (Meyer and Leidecker, 1999; Link et al., 2014); (3) lava damming by Columbia River Basalts (CRBs) and subsidence within the Columbia Basin (Reidel and Tolan, 2013; Larimer et al., 2019); and (4) uplift or mantle-lithospheric interactions (e.g., lithospheric delamination) associated with

Nate Mitchell https://orcid.org/0000-0002-2864-7952
[†]natemitc@indiana.edu

GSA Bulletin; November/December 2023; v. 135; no. 11/12; p. 3143–3162; https://doi.org/10.1130/B36524.1; 10 figures; 2 tables; 1 supplemental file.
Published online 16 March 2023

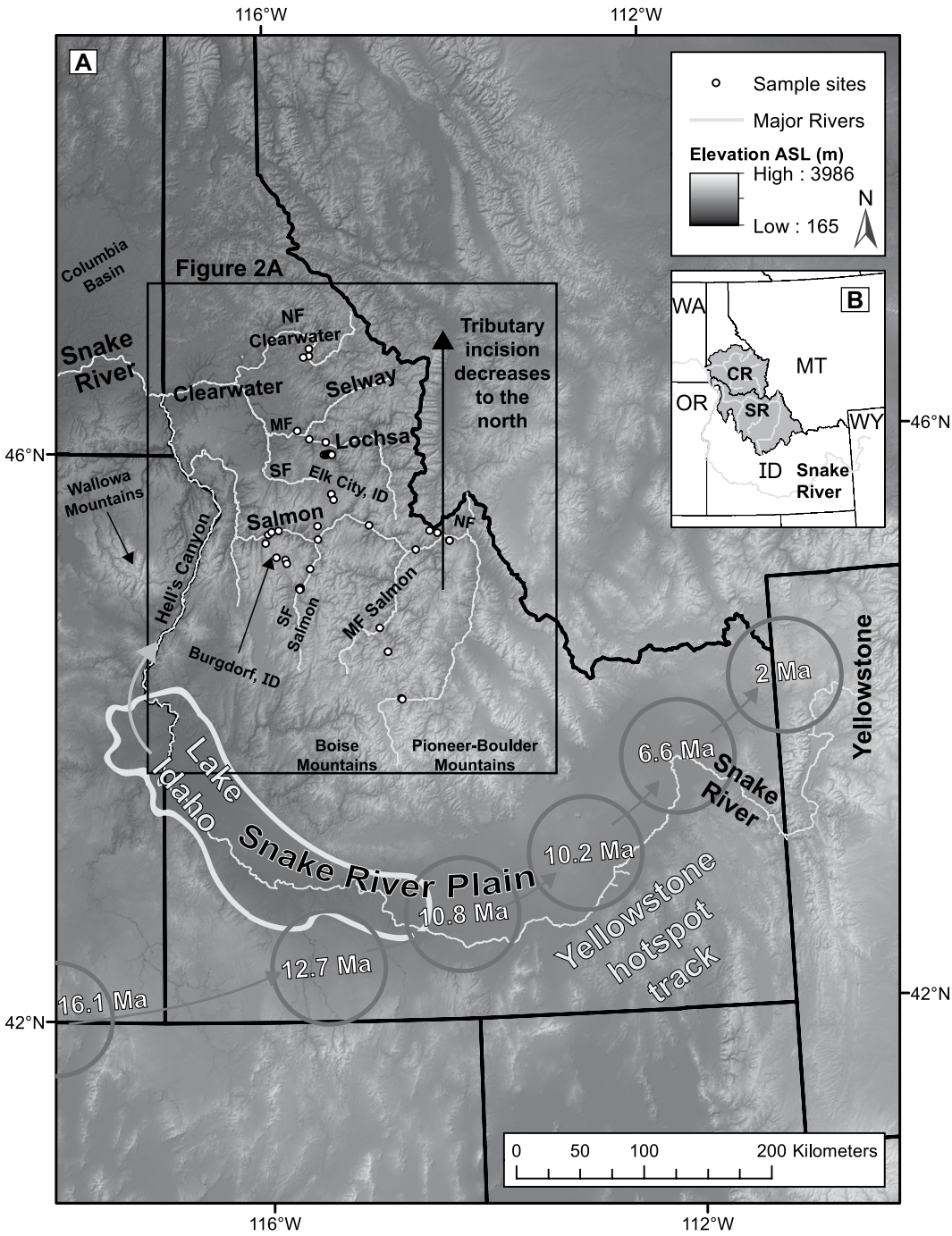

Figure 1. Figure adapted from Mitchell and Yanites (2019). (A) Overview of the study area in Idaho, USA. We investigate the drivers of transient incision along the Salmon and Clearwater rivers. We show (1) sampling locations for our cosmogenic erosion rates, (2) the former extent of Lake Idaho (Wood and Clemens, 2002), and (3) the Yellowstone hotspot track, with ages shown for previous caldera locations (Pierce and Morgan, 2009). (B) Inset showing the Salmon and Clearwater watersheds' positions within Idaho. State abbreviations are shown for Idaho (ID), Washington (WA), Oregon (OR), Montana (MT), and Wyoming (WY). The Salmon River and Clearwater River are labeled as SR and CR, respectively. NF—North Fork; MF—Middle Fork; SF—South Fork; ASL—above sea level.

the Yellowstone hotspot (Vogl et al., 2014; Larimer et al., 2019). These potential drivers are discussed in the background section below.

The foremost goal of this study is to use estimates of erosion rates and river incision modeling to test if the timing of canyon incision in central Idaho aligns with the expected timings for these hypotheses. Another goal of this study is to examine how landscape response depends on spatial variations in bedrock properties (Fig. 2A). Incision timing is influenced by the external forcing of a landscape as well as the properties of the landscape itself (e.g., bedrock erodibility), so constraining a landscape's history through river incision modeling requires careful consideration of how such properties are portrayed through model parameters.

Here, we apply a multifaceted approach to pursue the following research questions: (1) What is the spatial distribution of relict and adjusted erosion rates across the Salmon and Clearwater watersheds? (2) When did incision begin, and how does incision timing vary across the watersheds? (3) How do river incision model parameters such as erodibility vary with rock type and how do these parameters influence the reconstruction of geological history from topography? To address these research questions, we utilize 17 new and 29 previously published (Kirchner et al., 2001; Larimer et al., 2019) in situ ^{10}Be concentrations from fluvial sediment taken from the low-relief and high-relief (relict and adjusted, respectively) portions of central

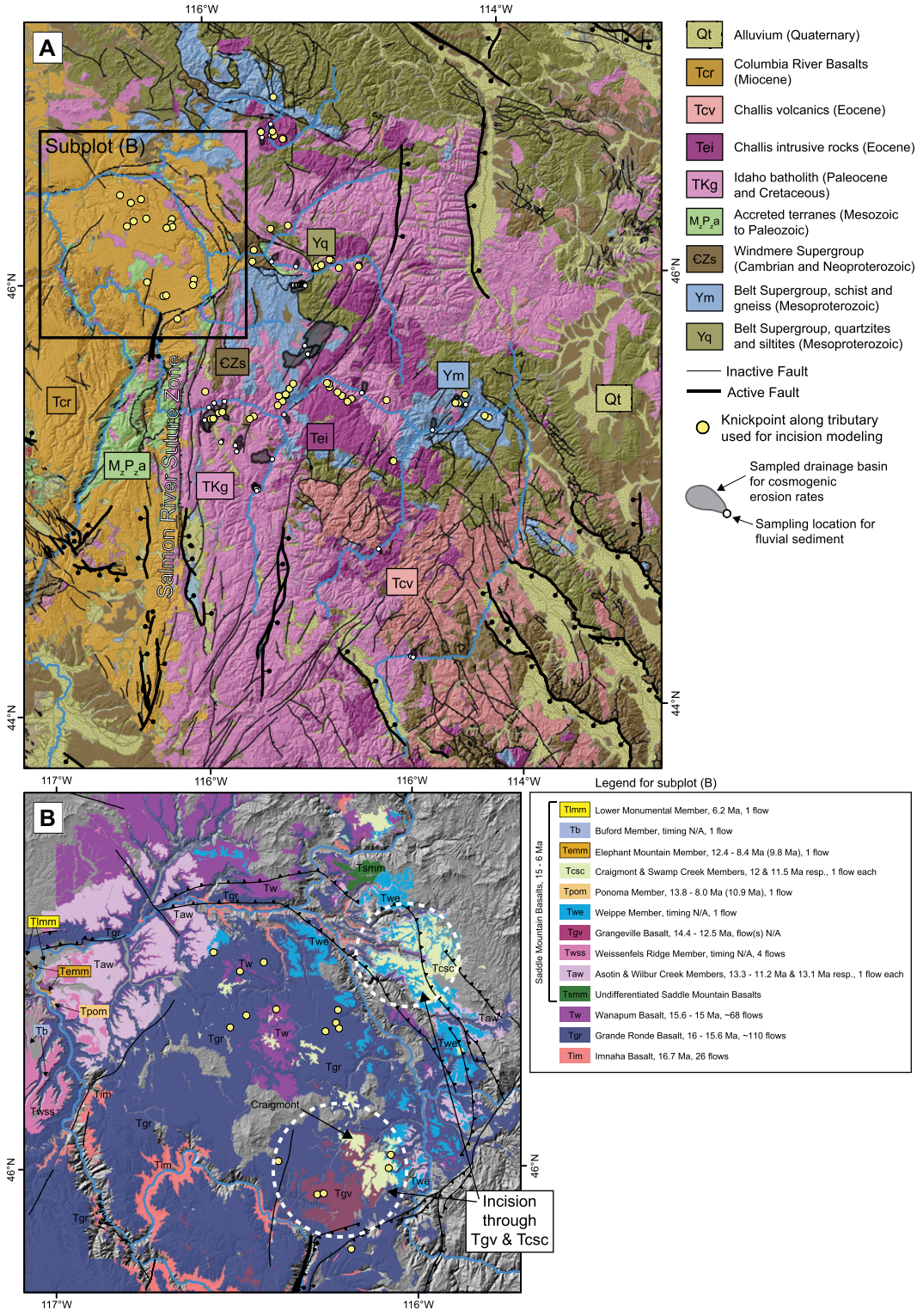

Figure 2. (A) Geologic map of the study area in northern Idaho, USA (see inset in Fig. 1A) (Lewis et al., 2012). Figure modified from Mitchell and Yanites (2019). (B) Columbia River Basalt flows underlying the basalt tributaries we study (Lewis et al., 2005, 2007; Kauffman et al., 2009; Barry et al., 2013; Reidel et al., 2013; Kauffman et al., 2014). Flow numbers and timings are from Barry et al. (2013); N/A stands for not available. Active faults (bold lines) are defined by the U.S. Geological Survey and Idaho Geological Survey (2018). Circles made of dashed white lines highlight the areas where tributaries have incised through the units Tgv (14.4–12.5 Ma) and Tcsc (12–11.5 Ma).

Idaho (Figs. 1A and 2A). We use these ^{10}Be concentrations and basalt geochronology to quantify erosion rates, calibrate stream power models, and estimate regional incision timing. Previous incision timing estimates in the region were spatially limited (Larimer et al., 2019), whereas we estimate incision timing for 57 new stream profiles distributed throughout the Salmon and Clearwater watersheds (Fig. 2A). Our study allows us to clarify the origin of landscape transience in the region and explore the relationships between lithology and bedrock river erosion.

BACKGROUND

Central Idaho Field Site

The complex geological history of this region allows for a large number of potential drivers of

TABLE 1. POTENTIAL DRIVERS OF TRANSIENT RIVER INCISION IN CENTRAL IDAHO, USA

Potential driver	Expected timing	Expected spatial pattern	References
Extensional collapse of a plateau	Sometime after ca. 67 Ma	Unclear; depends on collapse timing, orientation of major drainages during the collapse, and any resulting drainage reorganization.	Byerly et al. (2017); Fayon et al. (2017); Kahn et al. (2020)
Flood basalts cause lava damming, subsequent reincision, and (potentially) drainage reorganization	Between ca. 17 and 5 Ma	Incision within and upstream of areas underlain by basalt.	Larimer et al. (2018)
Subsidence of the Columbia Basin during flood basalt extrusion (although basalt infilling may inhibit the generation of base level fall)	Between ca. 17 and 5 Ma	By itself, we would expect it to generate uniform incision depths farther upstream (i.e., across central Idaho). Other factors could explain increased incision along the Salmon River.	Perry-Houts and Humphreys (2018)
Faulting along the Salmon River suture zone	During Basin and Range extension and after local CRB extrusion (Grande Rhonde basalt: 16–15.6 Ma), so potentially after ca. 15.6 Ma	Enhanced incision upstream of the faults along the Salmon River.	Tikoff et al. (2001); Barry et al. (2013); Kahn et al. (2020)
Lithospheric delamination	During the passage of the Yellowstone hotspot through Idaho, sometime after ca. 17 Ma	Enhanced rock uplift near the Idaho Batholith, decreasing with distance. Delamination would likely coincide with volcanism, and there are no recent volcanics in the batholith.	Larimer et al. (2018)
Lower crustal flow away from Snake River Plain	During the passage of the Yellowstone hotspot through Idaho, sometime after ca. 17 Ma	Enhanced rock uplift near the Snake River Plain (SRP), decreasing with distance. Potentially symmetric, with enhanced uplift on the north and south sides of the SRP.	McQuarrie and Rodgers (1998); Yuan et al. (2010)
Drainage of Lake Idaho down the proto-Snake River	Between ca. 3.4 and 2 Ma	Incision along the Snake River sweeps upstream into the Salmon and Clearwater rivers.	Wood (1994); Wood and Clemens (2002); Meyer and Leidecker (1999); Link et al. (2014); Staisch et al. (2021)

Note: CRB—Columbia River Basalts.

transient river incision. These potential drivers are summarized in Table 1. In this section, we discuss the region's geological history and each potential driver.

Much of central Idaho's tectonic history surrounds its position within the Cordilleran fold and thrust belt (Skipp, 1987; Link and Janecke, 1999; Janecke et al., 2000). Following the breakup of supercontinent Pangea in the Triassic, the North American Cordillera was built by subduction of oceanic crust and the accretion of intraoceanic island arcs to North America during the Mesozoic and early Cenozoic (Saleeby, 1983; Dickinson, 2004). Subduction of oceanic crust during this period created the Idaho Batholith (Fig. 2A; Skipp, 1987), with its first intrusions at ca. 98 Ma stitching the accreted terranes to North America along the Salmon River suture zone (Snee et al., 1984; Gaschnig et al., 2011). Sections of the Idaho Batholith continued to be emplaced until as late as 53 Ma (the Bitterroot lobe; Foster et al., 2001). Fabrics of the Atlanta lobe (83–67 Ma) of the Idaho Batholith suggest the presence of a crustal plateau (Byerly et al., 2017; Fayon et al., 2017), and the extension of such a plateau could be significant for regional exhumation (Kahn et al., 2020). Indeed, the creation of the Challis Magmatic Complex (Fig. 2A) during the Eocene (51–43 Ma) is thought to be related to the extensional collapse of over-thickened crust (Gaschnig et al., 2011).

Basin and range extension has been active in the far eastern regions of the Salmon Watershed from as early as 17 Ma to the present (Janecke et al., 1991; Janecke, 1992; Fig. 2A), but we do not study rivers in this area. In the western Salmon watershed, basin and range extension also reactivated the Salmon River suture zone (Tikoff et al., 2001) after the extrusion of the CRBs (Fig. 2); these basalt are discussed in greater depth below. The Salmon River suture zone had domino-style normal faulting (east-dipping faults, eastern side moving down) accommodating motion between the extending accreted terrain to the west and the intact Idaho Batholith to the east (Tikoff et al., 2001). This faulting generally does not extend into the batholith (Hamilton, 1963; Tikoff et al., 2001). The Quaternary fault database from the U.S. Geological Survey and Idaho Geological Survey (2018) does not indicate active faulting for most of the Clearwater and Salmon watersheds (active faults shown as bold lines in Fig. 2). Faulting along the Salmon River suture zone may have contributed to regional incision, but the east-dipping, east-side down normal faults would not have provided relative uplift in the upstream direction along the Salmon River. Regardless, any faulting related to the extensional collapse of a crustal plateau (Byerly et al., 2017; Fayon et al., 2017; Kahn et al., 2020) could still be important. For example, a reduction in elevation in one area could provide base level fall to areas farther upstream, potentially triggering transient incision and drainage reorganization. Furthermore, the Yellowstone hotspot is thought to have acted as a catalyst for Basin and Range extension (Parsons et al., 1994; Camp et al., 2015).

The western regions of our study area are unique lithologically, as they feature the CRBs. The timing of CRB extrusion from ca. 17 to 5 Ma over Oregon, Idaho, and Washington (USA) (Kasbohm and Schoene, 2018) generally coincides with the passage of the Yellowstone hotspot through southern Idaho (Fig. 1A; Reidel et al., 2013), and many studies have argued that the Yellowstone hotspot caused the extrusion of the CRBs (Camp, 1995; Dodson et al., 1997; Takahahshi et al., 1998; Camp and Hanan, 2008; Darold and Humphreys, 2013). Peak extrusion rates occurred from 16.7 to 15.9 Ma, generating over 95% of CRB volume (main eruptive phase; Reidel et al., 2013; Kasbohm and Schoene, 2018). Flood basalts filled river valleys, and the waning eruptions from ca. 15.6 to 6 Ma gave more time for rivers to incise through lava dams (Camp, 1981; Camp et al., 1982; Reidel et al., 2013). Lava damming could cause either a base level rise or a temporary decrease in base level fall rates, potentially creating the low-relief landscape in central Idaho (Larimer et al., 2019). Larimer et al. (2019) noted that once lava damming had ceased, the resumption of river incision could lead to the dissection of relict surfaces. Whether lava damming lasted long enough to drive a substantial decrease in relief within the relict surfaces remains an open question. Additionally, the Columbia Basin (Fig. 1A) subsided over 3.5 km between the onset and cessation of CRB volcanism (Reidel et al., 1989, 2013; Reidel and Tolan, 2013; Perry-Houts and Humphreys, 2018). This subsidence could drive base level fall in our study area, contributing to canyon incision. Infilling by basalt during subsidence would be an important consideration for the generation of base level fall, however.

Incision through dated lava flows provides maximum constraints on incision timing.

Figure 2B is a geologic map of the CRBs separated by flow age. The vast majority of CRBs here consist of the extensive Imnaha (ceased ca. 16.6 Ma; 5.3% of CRB volume), Grande Ronde (ceased ca. 16.1 Ma; 72.3% of CRB volume), and Wanapum basalts (ceased ca. 15.9 Ma; 5.9% of CRB volume; Barry et al., 2013; Kasbohm and Schoene, 2018). There are also thin units of the younger Saddle Mountain Basalts (ca. 15–6 Ma; 1.2% of CRB volume) in the area, which are composed of many small flows that became increasingly infrequent at ca. 12 Ma (Barry et al., 2013; Kasbohm and Schoene, 2018). Figure 2B shows that tributaries to the Salmon and Clearwater rivers have incised through the Grangeville (14.4–12.5 Ma), Craigmont (12 Ma), and Swamp Creek (11.5 Ma) members of the Saddle Mountain Basalts (Barry et al., 2013). We therefore argue that transient incision in this vicinity began after ca. 11.5 Ma. It is possible, however, that basalt extrusion occurred during ongoing regional incision. We will use incision timing estimates from nearby non-basalt tributaries to further assess this possibility, but the morphologies of basalt tributaries in Figure 2B can only attest to incision histories after ca. 11.5 Ma (i.e., the tributaries' morphologies were modified by extrusions until that time).

Canyon incision in central Idaho could also be related to the drainage of Lake Idaho. The lake occupied a fault-bounded graben in the western Snake River Plain (Fig. 1A) from ca. 9.5 to 1.7 Ma (Wood, 1994; Wood and Clemens, 2002). The lake's drainage area increased as the North American plate moved W-SW over the Yellowstone hotspot, forcing the continental divide farther eastward (Beranek et al., 2006; Wegmann et al., 2007). The lake's increasing drainage area contributed to it spilling over into what is now Hell's Canyon in western Idaho (Fig. 1A; Wood and Clemens, 2002). Wood and Clemens (2002) estimated this drainage to have occurred sometime between 6.4 and 1.7 Ma, but recent detrital U-Pb zircon data has further constrained the timing to between 3.4 and 2 Ma (Staisch et al., 2022). This drainage capture event may have caused incision along the Snake River, potentially sending a migrating wave of incision into the Salmon and Clearwater watersheds (Meyer and Leidecker, 1999; Link et al., 2014).

Larimer et al. (2019) argued that transient incision along the Salmon River could be related to interactions between the lithosphere and Yellowstone plume. Specifically, these authors hypothesized that the plume may have facilitated the delamination of a dense root from the aging Idaho Batholith (Fig. 2A). Such lithospheric foundering could replace eclogite with peridotite, generating surface uplift and river incision. By calibrating one-dimensional stream power models to transient stream profiles in a small area, these authors estimated that increased incision near Burdgorf, Idaho (Fig. 1A), began at ca. 9.5 ± 2 Ma. Interestingly, a threefold increase in exhumation rates from ca. 11 to 8 Ma is also shown by fission track data in the Boise Mountains (Fig. 1A; Sweetkind and Blackwell, 1989) and (U-Th)/He dating in the Pioneer-Boulder Mountains (Fig. 1A; Vogl et al., 2014). The style of northwards surface tilting proposed by Larimer et al. (2019) is further supported by a regional north-to-south gradient in canyon incision depths demonstrated by Mitchell and Yanites (2019). Incision depths along mainstem rivers increase by ~4 m per kilometer southwards (Fig. 1A), and the alignment of this incision gradient in relation to the Yellowstone hotspot track could suggest that the hotspot has played a role in canyon incision. Delamination within the Idaho Batholith would likely coincide with volcanism (Elkins-Tanton, 2007; Schoenbohm and Carrapa, 2015), however, and the absence of recent volcanics within the Idaho Batholith is notable. The Yellowstone hotspot could also provide uplift from thermal buoyancy (Vogl et al., 2014), but one might not expect such uplift to extend as far north as the Salmon and Clearwater rivers.

The Yellowstone hotspot could also drive regional surface uplift by emplacing mafic magmas (McQuarrie and Rodgers, 1998), which could then drive flexural uplift and/or induce lower crustal flow. For example, McQuarrie and Rodgers (1998) argued that the heavy load of a 17-km-thick, 100-km-wide basalt sill in the eastern Snake River Plain (in the Yellowstone hotspot track; Fig. 1A) may have driven lower crustal flow. Yuan et al. (2010) also argued that the magmatic loads of the eastern Snake River Plain could drive significant outflow of lower crust. The flow of the lower crust away from the eastern Snake River Plain could have inflated the surrounding crust, driving surface uplift and river incision. We would expect the surface uplift from lower crustal flow to be symmetrical on either side of the Snake River Plain, but only the north side has low-relief surfaces being dissected by incision (Fig. 1A). If lower crustal flow has contributed to surface uplift, either (1) the crust's structure made it energetically favorable for the lower crust to flow preferentially northwards or (2) Basin and Range extension south of the Snake River Plain has obliterated any evidence of previous surface uplift. One should also note that canyon incision driven by flexure and/or lower crustal flow is not dependent on a mantle plume model for the Yellowstone hotspot track, but only on the presence of basalt in the eastern Snake River Plain. For example, Zhou (2018) argued that the Yellowstone hotspot track represents the northeastward progression of tearing within the subducting Farallon slab, but this scenario would still emplace heavy loads of basalt within the Snake River Plain, potentially driving lower crustal flow.

The breadth of potential geologic processes influencing canyon incision in this region presents a rich problem. Indeed, this challenge highlights a wide variety of processes related to tectonics, geodynamics, volcanology, and drainage reorganization. Our focus is to use surface response (i.e., river incision) as a means of disentangling these drivers.

Background on Bedrock River Morphology and Erosion

We work to constrain the driver(s) of landscape transience in the northern U.S. Cordillera by analyzing the morphologies of bedrock rivers. Bedrock river incision is commonly represented by the stream power equation (Howard and Kerby, 1983; Howard, 1994; Whipple and Tucker, 1999):

$$\frac{\delta z}{\delta t} = U - KA^m \left|\frac{\delta z}{\delta x}\right|^n, \quad (1)$$

where z is elevation [L], t is time [T], U is rock-uplift rate [L T^{-1}], K is erodibility [L$^{1-2\,m}$ T^{-1}], A is drainage area [L^2], x is distance upstream [L], and both m and n are exponents. These exponents depend on erosion physics (Whipple et al., 2000a) and the scaling relationships between drainage area, channel width, and discharge (Whipple and Tucker, 1999).

If a stream is equilibrated ($dz/dt = 0$) and has uniform properties ($K \neq f(x)$), Equation 1 shows that channel slope (dz/dx) should scale with rock-uplift rates and erodibility:

$$\frac{dz}{dx} = \left(\frac{U}{K}\right)^{\frac{1}{n}} A^{\frac{-m}{n}} = k_s A^{\frac{-m}{n}}, \quad (2)$$

where k_s is channel steepness [L$^{2m/n}$] (Wobus et al., 2006). The ratio m/n influences river concavity θ (Tucker and Whipple, 2002), which describes the rate at which channel slope decreases with drainage area. The value of m/n is thought to vary from ~0.35 to 0.6 in graded rivers, although measured concavities can vary due to factors like the inclusion of transport-limited reaches or spatial changes in rock-uplift rates (Whipple and Tucker, 1999). Regressions of channel slope versus drainage area in log-log space (slope-area plots) can be used to quantify channel steepness (Wobus et al., 2006). Note that because the dimensions of k_s depend on

m/n, k_s values created with different m/n values cannot be directly compared. We therefore represent m/n with a reference concavity θ_{ref} and calculate a normalized steepness index k_{sn} as $|dz/dx| \times A^{\theta ref}$.

Separating variables in Equation 2 and integrating provides a method for depicting river profiles with a transformed distance upstream (Perron and Royden, 2013):

$$z = z(x_b) + \left(\frac{U}{KA_0{}^m}\right)^{\frac{1}{n}} \chi = z(x_b) + k_s A_0{}^{\frac{-m}{n}} \chi, \quad (3)$$

$$\chi = \int_{x_b}^{x} \left(\frac{A_0}{A}\right)^{\frac{m}{n}} dx, \quad (4)$$

where x_b is the position of base level ($x = 0$ m), χ is a transformed river distance upstream [L], and A_0 is a reference drainage area taken here as 1 km^2. River profiles displayed using χ rather than x are called χ-plots, and the gradient between river elevation and χ is related to channel steepness ($k_{sn} A_0{}^{-m/n}$).

Influence of Lithology on Fluvial Erosion

The combination of transient incision and complex geology in central Idaho also presents a valuable opportunity to explore the role of rock properties in fluvial erosion. Rock properties are known to have a significant influence on fluvial erosion and morphology (Goode and Wohl, 2010; Allen et al., 2013; Zondervan et al., 2020), but clear relationships between rock properties and river incision model parameters often remain elusive (Armstrong et al., 2021). The Salmon and Clearwater watersheds have a striking combination of lithologies that includes gneiss and quartzites of the Belt Supergroup, granodiorite of the Idaho Batholith, and the CRBs (Fig. 2A). Rock properties like fracture density (DiBiase et al., 2018; Scott and Wohl, 2019), tensile strength (Sklar and Dietrich, 2001; Bursztyn et al., 2015), and weathering susceptibility (Murphy et al., 2016; Ibarra et al., 2016) likely vary between the lithologies in central Idaho, and these properties influence fluvial erosion. Because our goal is to constrain the incision histories of tributaries to the Salmon and Clearwater rivers, we carefully consider both the influence of rock properties on incision model parameters and the influences of these parameters on the reconstruction of geological history from topography.

METHODS

We constrain the timing of canyon incision along 57 central Idaho tributaries using two approaches. First, we calculate tributary incision depths by projecting relict channel steepness from knickpoints to tributary outlets and then divide this incision depth by an estimated canyon deepening rate (i.e., incision rate; the difference between the adjusted and relict erosion rates). Second, we use calibrated stream power models to depict changes in river profiles through time. Incision timings are then estimated by comparing observed and simulated stream profiles. Below, we describe in detail our methods for quantifying erosion rates in relict and adjusted river basins and estimating incision timing.

Bedrock River Morphology and Erosion Rates

We used TopoToolbox v2 (Schwanghart and Kuhn, 2010; Schwanghart and Scherler, 2014) to extract river profile data from 10 m digital elevation models (DEMs) provided by the U.S. Geological Survey (USGS). We specifically extracted river profiles from transient drainage basins because transient stream profiles can be used to gain insight into past conditions (Whittaker, 2012). To minimize potential variations in rock strength, we only selected transient drainage basins underlain by a single lithology (granitoid, basalt, gneiss, quartzite, or siltite). Before analyzing river profiles, we manually selected a critical drainage area over 0.1 km^2 defining a "roll over" in slope-area data marking the transition from hillslope to fluvial processes (Montgomery and Foufoula-Georgiou, 1993). To minimize the noise common in DEMs (Wobus et al., 2006), we then smoothed river profile elevations over 55 nodes. We found this smoothing interval to reduce scatter in slope-area plots while preserving the shape of the profile. Because slope-area plots and χ-plots have different advantages and disadvantages (Wang et al., 2017), we used both methods to examine spatial variations in k_{sn} and identify sampling locations for our cosmogenic erosion rates. Using a reference concavity (θ_{ref}) of 0.5, we inspected slope-area plots and χ-plots to select the boundaries of relict and adjusted reaches. The boundaries of the relict and adjusted reaches were then used to calculate relict and adjusted steepness values within χ-plots (Equation 3).

For each transient tributary, we use Equation 3 to project the relict profile downstream of the knickpoint and estimate the incision depth at the tributary's outlet (Mitchell and Yanites, 2019):

$$I = z_{KP} - k_{snrel} A_0{}^{\frac{-m}{n}} \chi_{KP} - z(x_b), \quad (5)$$

where I is incision depth [L], z_{KP} is knickpoint elevation, $k_{sn\ rel}$ is the relict steepness, χ_{KP} is the χ value at the knickpoint, and $z(x_b)$ is the outlet elevation (i.e., the tributary's confluence with the mainstem river). The resulting incision depth can be regarded as the thickness of extra rock the tributary has eroded through during its transient adjustment (in comparison with the thickness of rock eroded in the relict part of the landscape). Because we focus on small tributaries underlain by single rock types, our approach minimizes the uncertainties involved in projecting the relict steepness to the tributary outlet (e.g., limited climatic and lithologic variability over such short distances). We estimated incision depths in χ-plots created with reference concavities (i.e., m/n ratios in Equation (5)) of 0.3, 0.5, and 0.7.

Calculating Cosmogenic Erosion Rates

Cosmogenic radionuclides (CRN) are created when cosmic rays impact nuclei, causing spallation reactions in which lighter nuclei are ejected (von Blanckenburg, 2005). The production rate of CRNs within soil and bedrock decreases with depth due to the scattering and absorption of cosmic rays (Gosse and Phillips, 2001). The accumulation of CRNs in bedrock is also offset by their removal at the surface through erosion, and in an equilibrated landscape this competition leads to a characteristic CRN concentration at the bedrock surface (Lal, 1991). The approach commonly taken by geomorphologists (Bierman and Steig, 1996; Granger et al., 1996) is to sample fluvial sediment in an active channel and use the CRN concentration of the sediment to represent the average concentration within bedrock surfaces upstream of the sampling location. The CRN we focus on here, ^{10}Be, accumulates in quartz, so we sampled fluvial sediment from drainage basins underlain by quartz-bearing lithologies.

We collected fluvial sediment at 17 locations within the Salmon and Clearwater watersheds (Figs. 1A and 2A). These locations were selected to isolate a completely relict (low erosion rate) or adjusted (high erosion rate) drainage basin lacking any indication of recent landslides or glaciation. Rather than sampling mainstem rivers that integrate a multitude of lithologies and erosional signals, we targeted smaller tributaries (0.74–10 km^2) to minimize variations in lithology and erosion rate. We selected five sampling locations in what we interpreted to be the relict landscape and 12 locations in what we interpreted to be the adjusted landscape. We based these interpretations on spatial patterns in channel steepness and hillslope angle distributions. The sampling locations were also selected to complement previously published CRN-derived erosion rates in this region (Kirchner et al., 2001; Larimer et al., 2019).

After collecting sediment samples in the field, we cleaned and separated the quartz grains

using the methods of Kohl and Nishiizumi (1992). We then isolated the beryllium in the quartz and measured ^{10}Be concentrations at the PRIME Laboratory at Purdue University. With these in situ ^{10}Be concentrations, we then calculated catchment-averaged erosion rates using LSDTopoTools (Mudd et al., 2016) and a 10 m DEM provided by the USGS. In LSDTopoTools, we filled the DEM using a minimum slope of 0.0001, calculated topographic shielding using an azimuth interval of 5° and an inclination interval of 5° (as recommended by Codilean, 2006), and chose the Braucher et al. (2009) scaling scheme for CRN production by muon-induced reactions. To assess the impact of topographic shielding on these erosion rates (DiBiase, 2018), we also calculated erosion rates without topographic shielding.

We combined the results for these 17 new samples with those for 29 samples from previous studies (21 from Kirchner et al., 2001, and eight from Larimer et al., 2019). We processed the ^{10}Be concentrations for these 29 samples in LSDTopoTools in the same manner described above. We interpreted that 18 of the samples are in relict drainage basins, eight of the samples are in adjusted drainage basins, and three are in transient drainage basins (i.e., containing both relict and adjusted portions). With these 29 additional samples, we used a total of 46 samples in this study (Figs. 1A and 2A). This compilation resulted in 23 relict, 20 adjusted, and three transient samples in our analysis. The three transient samples are not used in the determination of relict and adjusted erosion rates.

Estimating Incision Timing from Incision Depths and Rates

Whereas we used relict and adjusted drainage basins to constrain the relict and adjusted erosion rates in central Idaho, we used the stream profiles of transient drainage basins to constrain incision timing. We examined the transient incision of streams that drain directly into large drainages: the Salmon, Middle Fork Salmon, Clearwater, Middle Fork Clearwater, North Fork Clearwater, Selway, and Lochsa rivers (Fig. 1A). We focused on small tributaries because the incision at their outlets represents the incision of the mainstem river they flow into. This approach therefore allowed us to use main-stem rivers as a datum while also benefitting from the reduced uncertainty within individual transient tributaries. For example, these small tributaries (1) allow for minimized climatic and lithologic variability and (2) help us to avoid complications from long-wavelength patterns in rock uplift.

Incision timing is estimated using the incision depths (I) measured for each tributary (Equation 5). Specifically, we calculate an incision timing as:

$$t_I = \frac{I}{E_{adj} - E_{rel}}, \quad (6)$$

where t_I is incision timing [T] and E_{adj} and E_{rel} are adjusted and relict erosion rates [L T^{-1}], respectively. We assess two sets of values for E_{adj} and E_{rel}. The first set is based on the average adjusted and relict cosmogenic erosion rates. The second set is intended to portray a maximum incision rate, which would provide a minimum timing (t_I). The maximum incision rate uses the highest E_{adj} value and the lowest E_{rel} value, where each value is defined analyzing our adjusted and relict cosmogenic erosion rates (described below and in the Supplemental Material[1]). We do not use a minimum incision rate (utilizing the lowest E_{adj} and highest E_{rel}, providing a maximum incision timing) because we will show that there is some overlap between the ranges of relict and adjusted erosion rates from different tributary basins. This overlap occurs in part because of the considerable uncertainty inherent in the use of cosmogenic erosion rates.

Bedrock River Incision Models

To define the range of base level fall rates in our incision models, we created a normal probability density function (PDF) for each relict and adjusted cosmogenic erosion rate. We used these PDFs to evaluate the probability that each erosion rate occurs within different intervals (spacings of 0.005, 0.010, and 0.015 mm yr^{-1}). We then used the probabilities from all samples to define the lower and upper limits for relict and adjusted erosion rates in our incision models. Further details on this approach can be found in the Supplemental Material.

We use the stream power model to simulate tributary incision over time. The incision approach described in the previous section relies on the projection of relict profiles with steepness regressions. However, our simulations of bedrock river incision over time are meant to estimate incision timing without strict assumptions regarding the initial conditions. In other words, if a simulation can sufficiently replicate the observed transient stream profile within a parameter space we define as reasonable, then we accept the incision timing from that model as being potentially representative of the transient tributary in question. Furthermore, the calibration of incision models to tributaries from different rock types will allow us to explore the relationships between lithology and incision model parameters. The transient responses of bedrock rivers are a critical test for models of fluvial erosion (Whipple, 2004), and the substantial transient incision in central Idaho provides an excellent opportunity to explore how the transient behavior of bedrock rivers varies with rock type. Such information is not offered by our first approach for estimating incision timing.

We simulated the transient response of a river profile to a change in base level fall rates over 34 m.y. The base level fall rates change from an initial rate (U_i) to a final rate (U_f), and t is the time since the change occurred. We calculate river profiles every 0.1 m.y. from 0.1 to 34 m.y.; more details regarding this approach are provided further below. The relict portion of the landscape is in steady-state with U_i, while the adjusted portion will eventually be in steady-state with U_f. By comparing simulated and observed profiles over time, one can estimate when transient incision began. For example, if transient incision began at 7 Ma then the simulated profile at $t = 7$ m.y. should have the lowest misfit relative to the observed profile (if the model and its parameters are accurate and representative). We chose to use a maximum time of 34 m.y. (i.e., from the beginning of the Oligocene to the present) because it more than encompasses the main events we focus on as potential drivers of transient incision in the region: the drainage of Lake Idaho at ca. 3.4–2 Ma (Staisch et al., 2022) and the onset of hotspot volcanism near southeastern Oregon at ca. 17–16 Ma (as well as related events, like the Yellowstone hotspot's passage through southern Idaho, CRB volcanism, and the reactivation of the Salmon River suture zone; Pierce and Morgan, 1992; Tikoff et al., 2001; Camp and Hanan, 2008; Pierce and Morgan, 2009; Camp et al., 2015). Although transient incision could be related to the extensional collapse of a crustal plateau sometime after the emplacement of the Atlanta lobe of the Idaho Batholith (83–67 Ma; Byerly et al., 2017; Fayon et al., 2017), we do not assess model times approaching 67 Ma for the following reasons: (1) the exact timing of extensional collapse is poorly defined, (2) it is far less likely the drainage networks we study are representative of those existing as early as 67 Ma, and (3) such early times are well beyond the creation of several units underlaying the tributaries we examine (the Eocene Challis intrusive granitoids and the CRBs; Fig. 2A). Although we assess incision models for basalt tributaries up to 34 m.y., the morphologies of rivers underlain by

[1]Supplemental Material. Text: Probability Distributions for Relict and Adjusted Erosion Rates. Figures S1–S30. Tables S1–S2. Please visit https://doi.org/10.1130/GSAB.S.21677063 to access the supplemental material, and contact editing@geosociety.org with any questions.

TABLE 2. PARAMETER SPACE FOR BEDROCK RIVER INCISION MODELS, CENTRAL IDAHO, USA

Parameter	Value
dt (m.y.)	0.1
t_{max} (m.y.)	34
Evaluated K values/calculated K	0.75, 0.9, 0.95, 0.98, 1, 1.02, 1.05, 1.1, and 1.25
Maximum proportional change in K for convergence	0.02
A_0 (km^2)	1
Slope exponent n	0.5, 0.6, 0.67, 0.75, 1, 1.33, 1.5, 1.67, 2, and n_{calc}
θ_{ref}	0.3, 0.5, and 0.7
Drainage area exponent m	$n\ \theta_{ref}$
U_i range (mm yr^{-1})	0.02 to 0.06
U_f range (mm yr^{-1})	0.04 to 0.11
U interval (mm yr^{-1})	0.005

the CRBs (Fig. 2B) clearly cannot attest to incision that precedes the basalt itself.

We used the analytical version of the stream power model (Royden and Perron, 2013; Mitchell and Yanites, 2019) to simulate river profile evolution following a step change in base level fall rates. The parameter space for our incision models is summarized in Table 2. Because we use an analytical approach, there are no initial conditions; using the χ values calculated for each tributary (Equation 4), a transient profile can simply be calculated for any given time t based on the assumed base level fall rates (initial rate U_i and final rate U_f) and stream power model parameters (K, n, and m) in each scenario. Because we do not use a finite difference approximation, our models have no stability requirements and lack the numerical diffusion that occurs with the first-order upwind finite difference approximations commonly used for the stream power model (Royden and Perron, 2013). Although we did not use a forward-running numerical model, our approach is similar in that we calculate a profile every 0.1 m.y. from 0.1 to 34 m.y. (all within one combination of K, n, m, U_i, and U_f). After finding a best-fit model time within that combination of K, n, m, U_i, and U_f we calculate profiles over time for the next combination of model parameters. Note that for visual clarity in our figures, the main text only includes results for $\theta_{ref} = 0.5$. Results for reference concavities of 0.3 and 0.7 did not change our general conclusions but are included in the Supplemental Material to illustrate sensitivity to this parameter choice.

We use the X^2 Misfit Function to compare observed and simulated stream profiles (Jeffery et al., 2013):

$$X^2 = \frac{1}{N - \nu - 1} \sum_{i}^{N} \left(\frac{sim_i - obs_i}{tolerance} \right)^2, \quad (7)$$

where X^2 describes the average misfit between the observed and simulated river profiles, N is the number of nodes along the profile, ν is the number of free parameters, sim_i is the simulated river elevation at node i, obs_i is the observed river elevation at node i, and *tolerance* is a length scale we discuss below [L]. Because we only vary K for each combination of n and m (variation of these exponents is described below), we set ν to one. In the Supplemental Material, we present a method for calculating *tolerance* based on the average differences between steepness-derived elevations and observed elevations. The results shown in the main text use a *tolerance* of 30 m to represent the average *tolerance* value calculated for transient stream profiles (29.3 m for $m/n = 0.5$; average *tolerance* values calculated with $m/n = 0.3$ and $m/n = 0.7$ are 44.8 m and 34.1 m, respectively). We also show results where *tolerance* varies (as calculated for each tributary) in the Supplemental Material. We focus on results where *tolerance* is always 30 m in the main text to maintain a uniform treatment for all transient stream profiles.

The slope exponent n parameter (Equation 1) has a significant impact on the transient response of a bedrock river (Tucker and Whipple, 2002). Although scaling analyses of erosion processes like plucking and abrasion suggest n ranges from ~0.67 to 1.67 (Whipple et al., 2000a), studies have reported n values as low as 0.4 ± 0.2 (Whipple et al., 2000b) and ~0.5 (Gallen and Wegmann, 2017) as well as n values as high as 2.43 ± 0.15 (Harel et al., 2016) and ~7 (Gallen and Fernández-Blanco, 2021). Our models incorporate a wide range of reference slope exponent n values (0.5–2; Table 2). Because (1) n controls whether a particular combination of U_i and U_f can reproduce the observed change in steepness between relict and adjusted reaches and (2) we cannot confidently define limits for this parameter, we also evaluated simulations for a calculated n value (n_{calc}). In each combination of U_i and U_f, we calculated an n_{calc} value as (Duvall et al., 2004):

$$n_{calc} = \frac{log\left(\frac{U_f}{U_i}\right)}{log\left(\frac{k_{snadj}}{k_{snrel}}\right)}, \quad (8)$$

where $k_{sn\ adj}$ and $k_{sn\ rel}$ are the steepness values of the adjusted and relict reaches measured in χ-plots, respectively. The n_{calc} produced with Equation 8 is the n value required to achieve the observed change in steepness ($k_{sn\ adj} / k_{sn\ rel}$) for a given combination of U_i and U_f. For each value of n, we calculate drainage area exponent m as $n \times \theta_{ref}$.

Every tributary has a suite of simulations for each combination of U_i, U_f, slope exponent n, and drainage area exponent m in which we optimize erodibility K. This optimization consists of evaluating different simulations using erodibilities distributed around the K value initially calculated as:

$$K = U_f k_{sn\ adj}^{-n}. \quad (9)$$

The different simulations assess K values ranging from 75% to 125% (Table 2) of the K calculated with Equation 9. After running each simulation, the K that produces the lowest misfit is made the center of a distribution of K values for a new set of simulations. This process of finding a best-fit K and then exploring erodibilities distributed around that best-fit K value continues until the proportional change in the best-fit K between one set of simulations and the next is less than or equal to 2%. Erodibility optimization occurs for each simulation from $t = 0.1$ m.y. to $t = 34$ m.y., and the computational efficiency of the analytical stream power model aids in handling such a large number of simulated profiles. We chose to optimize K because there is considerable uncertainty in U, m, and n; if a slight change in K can mean the difference between an acceptable or unacceptable model, our intention is to allow that change in erodibility. By optimizing K, our intention was also to test the accuracy of Equation 9 for the calibration of incision models. Equation 9 only uses an adjusted k_{sn} for a particular set of assumed U and n values, but a best-fit K must reflect the entire profile (e.g., relict k_{sn} and the shape of the knickzone). We present the changes between the initial K (Equation 9) and the final best-fit K values in the Supplemental Material.

We defined a simulation as being acceptable when it has a $X^2 \leq 1$ (Equation 7). A X^2 value is the average difference in observed and simulated elevations, which is then divided by the *tolerance* and squared. With a *tolerance* of 30 m in our main simulations, having $X^2 \leq 1$ means that a simulated profile is within 30 m of the observed profile, on average. Because we optimized K in each simulation and thoroughly explored the parameter space (U_i, U_f, n, and m), we argue that our definition of an acceptable model is conservative, allowing a broad range of potential landscape transience histories.

RESULTS

Bedrock River Morphology

Within the studied tributaries, we consistently observe low-steepness reaches at high elevations and high-steepness reaches at low elevations (Fig. 3). These observations are consistent with our interpretation of central Idaho as a transient landscape (Mitchell and Yanites, 2019). Many tributaries have broad, convex knickzones (Fig. 3C) that we interpret as stretch zones (Royden and Perron, 2013) situated between relict and adjusted reaches. In contrast, basalt tributaries generally lack a convex knickzone and instead have sharp knickpoints (Fig. 3B). The tributaries in Figure 3 are distributed across the study area, with their locations shown in inset maps. In each subplot, we show the incision depths estimated by projecting the relict steepness (dotted lines) from the knickpoint to the tributary's outlet (Equation 5). The incision depths of these three tributaries range from ~360 m to ~1 km and are consistent with the north-to-south gradient in incision depths reported by Mitchell and Yanites (2019).

Cosmogenic Erosion Rates

Figure 4 shows the sampled drainage basins colored by erosion rate. These samples are widely distributed across these watersheds, extending from the North Fork Clearwater River to the upper reaches of the Salmon River. Erosion rates range from ~0.024 mm yr^{-1} to 0.105 mm yr^{-1}. Assuming an absorption depth scale of 0.6 m, these cosmogenic erosion rates would represent timescales of ~5.7–25 k.y. (absorption depth scale/erosion rate; Brown et al., 1992; Bierman, 1994). Tables S1 and S2 (see footnote 1) provide more details regarding cosmogenic erosion rate calculations (e.g., sample latitude, longitude, and ^{10}Be concentrations). These tables also include the erosion rates calculated with and without topographic shielding. Topographic shielding has a minimal impact on the calculated erosion rates, with almost all values changing by less than 2%. Only two samples had changes in erosion rate exceeding 2%: one value changed by 2.27% (unnamed Middle Fork Salmon tributary) and another changed by 11.76% (White Creek). The erosion rates shown in Figures 4 and 5 were calculated with topographic shielding.

Figures 5A and 5B show all cosmogenic erosion rates relative to reference frame a-b-c-d, which is shown in Figure 4A. Conversely, Figures 5C and 5D show sample locations with distances upstream from the Salmon and Clearwater watershed outlets, respectively, and only for tributaries directly connected to mainstem rivers. Erosion rates vary between the relict and adjusted catchments, with relict erosion rates ranging from ~0.024 to 0.061 mm yr^{-1} and adjusted erosion rates ranging from ~0.05 to 0.105 mm yr^{-1}. Figure 5 shows there is no clear spatial trend in these data. Instead, relict and adjusted erosion rates in both watersheds vary around mean values. The mean relict and adjusted erosion rates of 0.037 ± 0.0098 mm yr^{-1} and 0.076 ± 0.017 mm yr^{-1} (with uncertainties representing standard deviation) are shown as dotted and dashed lines in Figures 5A and 5B (E_{rel} and E_{adj}). For an absorption depth scale of 0.6 m, these average relict and adjusted erosion rates would represent timescales of ~16.2 k.y. and 7.9 k.y., respectively (Brown et al., 1992; Bierman, 1994). The mean relict and adjusted erosion rates are similar along both the Salmon River (Fig. 5C) and Clearwater River (Fig. 5D). Note that the mean erosion rates listed above include erosion rates from basins situated within other, larger basins being used (Figs. 4E–4G). If the erosion rates from the smaller basins are excluded so that only the erosion rates from the larger basins are used, the average relict and adjusted erosion rates are ~0.041 and 0.071 mm yr^{-1}, respectively. Because of the considerable uncertainty inherent in cosmogenic erosion rates, we argue that these average relict and adjusted erosion rates are quite similar to our overall averages of 0.037 and 0.076 mm yr^{-1}.

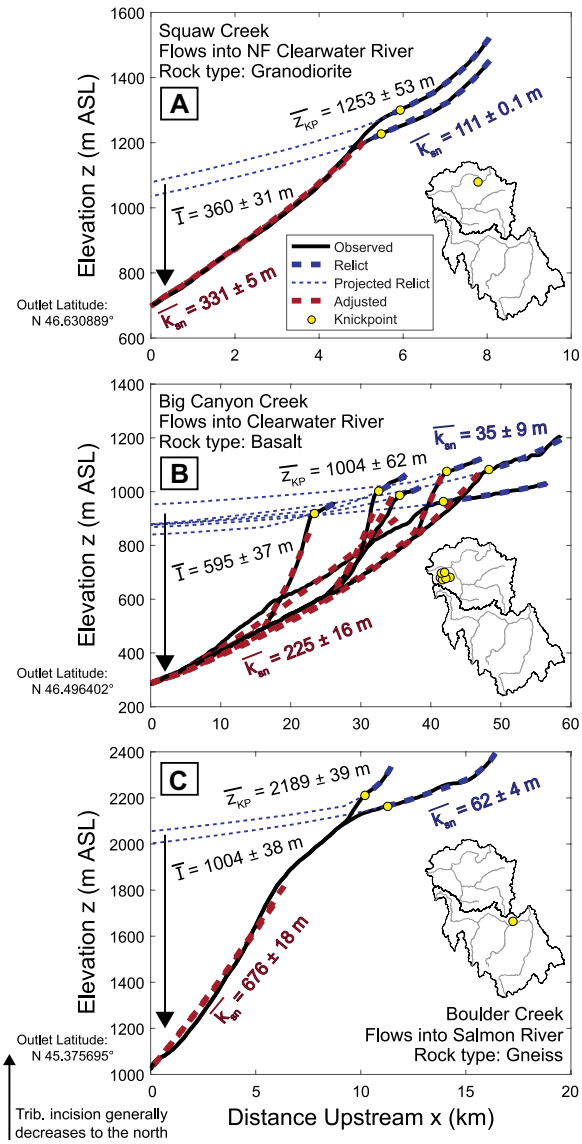

Figure 3. Long profiles demonstrating the distribution of transient incision across the Salmon and Clearwater watersheds in Idaho, USA. We show knickpoint elevations (z_{KP}, yellow circles), steepness values (k_{sn}) of relict and adjusted reaches (blue and red, respectively), and estimated incision depths (I). The location of each stream is shown in an inset map. NF—North Fork; trib.—tributary; m ASL—meters above sea level.

Base Level Fall Rates in River Incision Models

We use these erosion rates to establish the base level fall rates in our two approaches for estimating incision timing (i.e., dividing incision

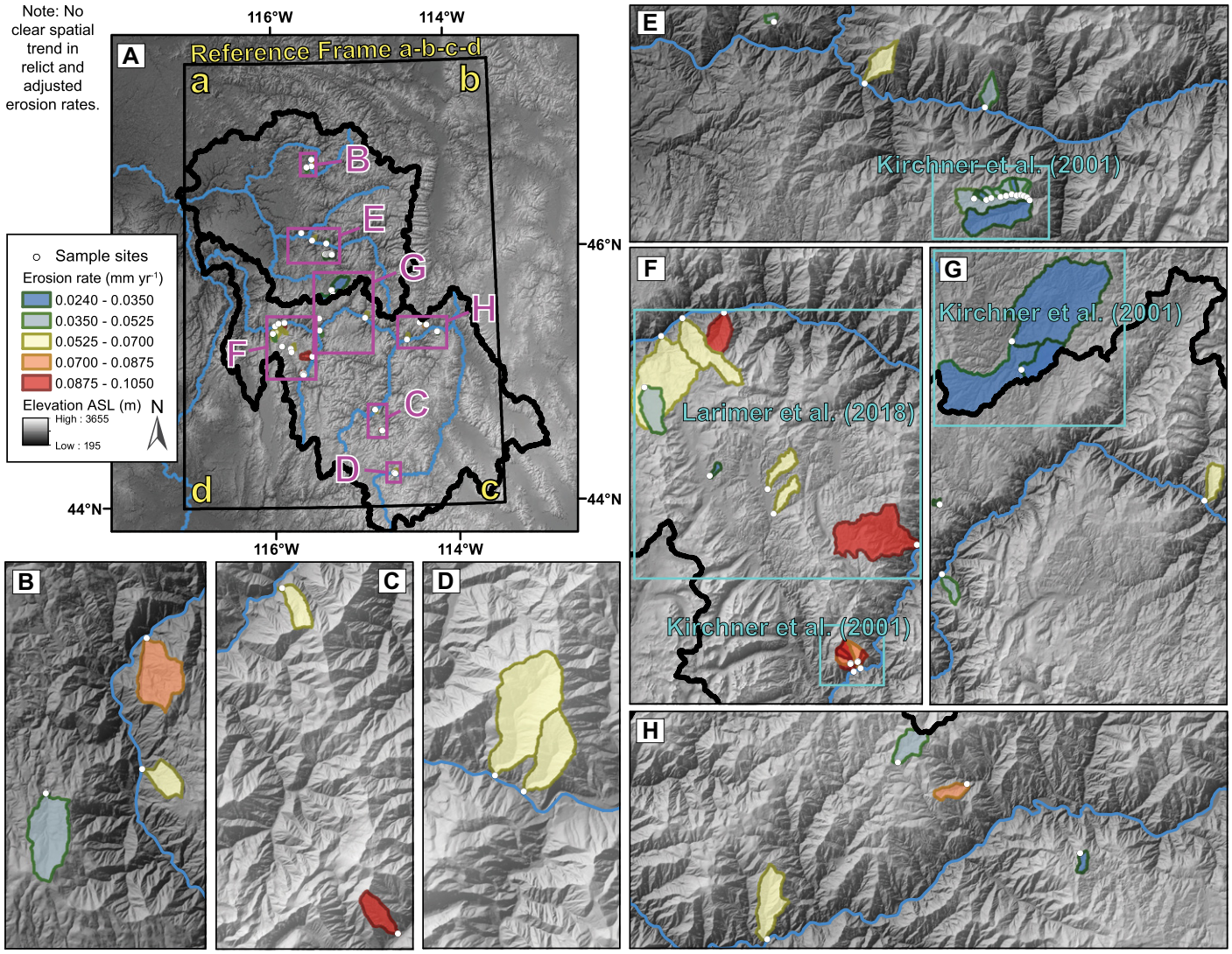

Figure 4. Overview of the cosmogenic erosion rates in this study (Idaho, USA). Reference frame a-b-c-d in subplot A is used in Figures 5 and 11. The samples from Kirchner et al. (2001) and Larimer et al. (2019) are labeled in subplots E–G. ASL—above sea level.

depths by incision rates and simulations over time). By evaluating probability distributions for our entire collection of relict and adjusted erosion rates (Figs. S1 and S2), we defined the ranges of initial (U_i) and final (U_f) base level fall rates as 0.02–0.06 mm yr^{-1} and 0.04–0.11 mm yr^{-1}, respectively (Fig. 5). Given these ranges, in our first approach for estimating incision timing (Equation 6) we estimate incision timings with $E_{rel} = 0.037$ mm yr^{-1} and $E_{adj} = 0.076$ mm yr^{-1} as well $E_{rel} = 0.02$ mm yr^{-1} and $E_{adj} = 0.11$ mm yr^{-1} (where the latter set provides a minimum incision timing). In our second approach for estimating incision timing (i.e., simulations over time), we vary U_i and U_f values with an interval of 0.005 mm yr^{-1} (Table 2). Because there is overlap in the ranges for U_i and U_f, we only assess incision models where $U_i < U_f$.

Incision Timing Estimates from Incision Depths and Rates

Incision timings from Equation 6 using the average relict and adjusted erosion rates (large symbols in Fig. 6) suggest transient incision began between 20.6 and 8.5 Ma in the Clearwater watershed and 30.8–13.1 Ma in the Salmon watershed. Upstream of the basalt along the Salmon River, minimum incision timings were calculated at ca. 10 Ma (small symbols in Fig. 6B). For the basalt tributaries along the lower Salmon River (farther to the north), minimum incision timings were calculated at ca. 6 Ma. Throughout the Clearwater watershed, minimum incision timings were generally calculated at ca. 5 Ma (Fig. 6A). This northwards decrease in estimated incision timing is captured by the regressions shown in Figure 7A ($R^2 = 0.68$). There is also a slight decrease in estimated incision timing from east to west (Fig. 7B). These findings are also supported by results using reference concavities of 0.3 and 0.7 (Figs. S4–S7).

Best-Fit Bedrock River Incision Models

Example best-fit incision models are presented in Figure 8 (Salmon River) and Figure S8 (Clearwater watershed). These models demonstrate that our definition of an acceptable model (i.e., a *tolerance* of 30 m) generally allows us to differentiate between simulations that would be visually described as good or poor model fits. For each tributary in Figure 8, we show incision models using three selections

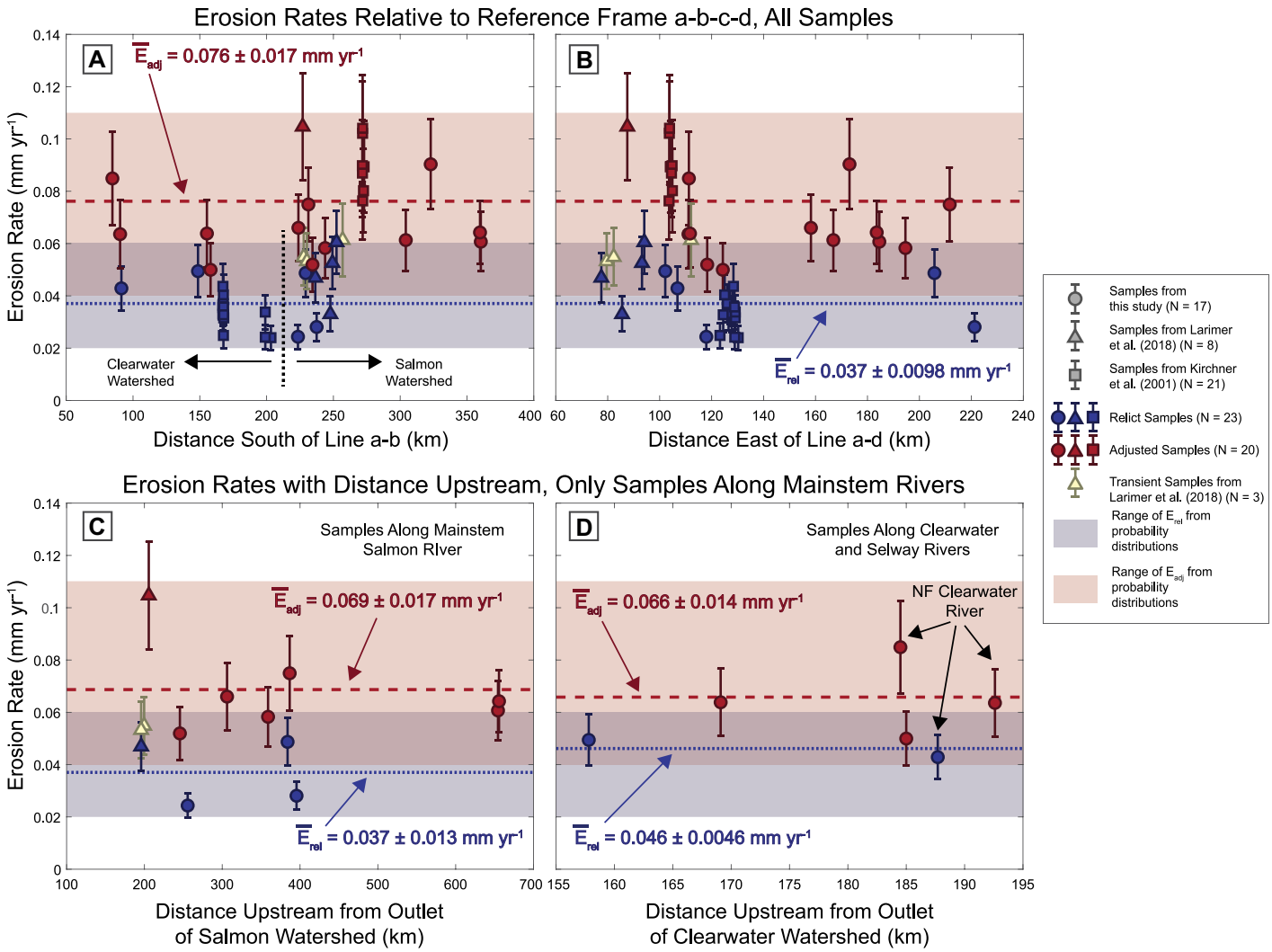

Figure 5. Cosmogenic erosion rates used in this study (Idaho, USA). Subplots A and B show all samples' positions (A) with distance south of line a-b and (B) with distance east of line a-d (Fig. 4A). Subplot C shows only samples situated along the Salmon River while subplot D shows only samples situated along the Selway, Middle Fork Clearwater, and North Fork Clearwater rivers. The error bars on each erosion rate represent the total error (as reported by LSDTopoTools). Average adjusted (E_{adj}) and relict (E_{rel}) erosion rates are shown with standard deviations.

of slope exponent n: (1) a calculated n (Equation 9), (2) a reference n value of 1, and (3) a reference n value of 2. For the U_i and U_f values used in these examples (0.03 and 0.09 mm yr^{-1}), the calculated n values range from 0.55 to 0.75. These low n values produce excellent model fits, while the higher n values of 1 and 2 often lead to poor model fits. Higher n values generally fail to produce the large changes in steepness between relict and adjusted reaches. Furthermore, many streams in this region feature broad, convex knickzones (e.g., Carey Creek and Golden Creek in Fig. 8) that are only reproduced by models with $n < 1$ (Royden and Perron, 2013). Across all of our models, n_{calc} values of acceptable models range from 0.040 to 2.47 while median n_{calc} values are generally between 0.4 and 0.6. More details regarding the parameters of our incision models (performances of the n_{calc} and reference n values) are available in the Supplemental Material.

Figure 9 shows the estimated incision timings for all 23,654 acceptable models within the Clearwater watershed (Figs. 9A–9D) and Salmon watershed (Figs. 9E–9H). Because we show a broad range of potential landscape histories here, one should focus on the overlap between tributaries' minimum and maximum incision timings (i.e., nearby tributaries should have similar incision histories). In each 50 km section of Figure 9, we show the overlap between the section's highest minimum and lowest maximum incision timings, which are generally acceptable incision timings for all tributaries in that section (those with any acceptable models).

Simulations using higher n values can produce relatively recent incision timing estimates (e.g., up to 1.5 and 2.4 Ma for $n = 2$ in Figs. 9D and 9H). These models with high n values, however, fail to produce any acceptable models for a large proportion of tributaries (especially along the Salmon River). In contrast, models with lower n values (e.g., $n = 0.67$ in Figs. 9B and 9F) more consistently produce acceptable models, and these models have earlier incision timings. Indeed, along the deeply incised section of the Salmon River (upstream of the basalt) the overlapping ranges of timings from both models using $n = 0.67$ (Fig. 9F) and models using all n values (Fig. 9E) suggest transient incision began

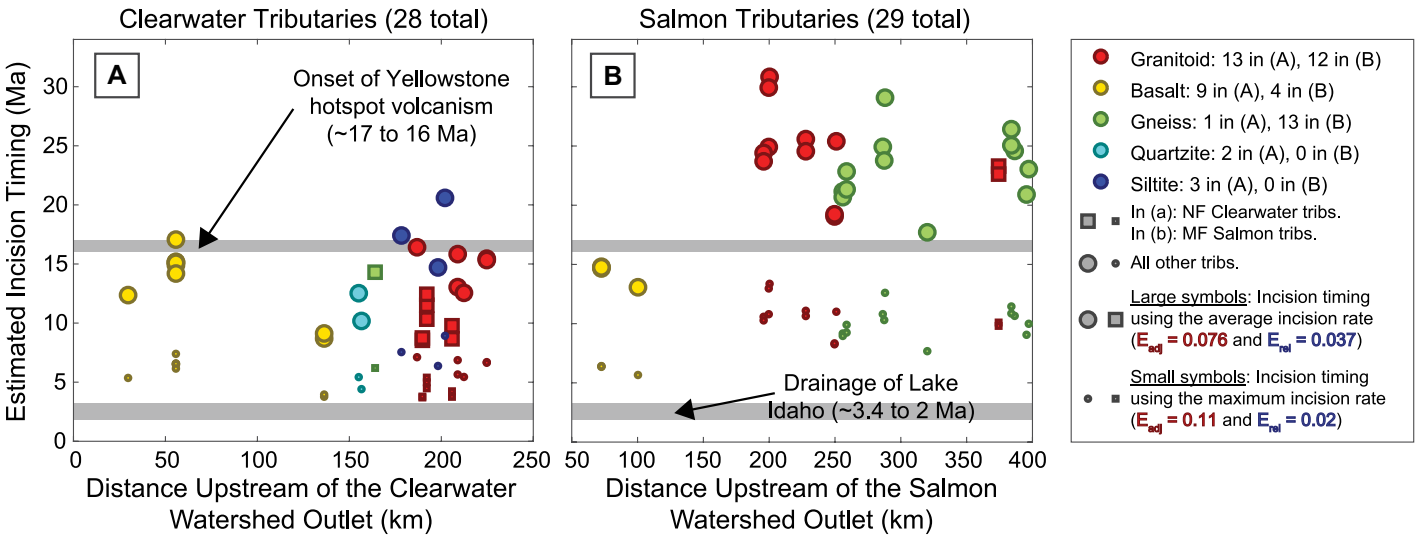

Figure 6. Estimated incision timings shown by each tributary's (tribs.) distance upstream of the (A) Clearwater watershed outlet and (B) Salmon watershed outlet (Idaho, USA). NF—North Fork; MF—Middle Fork; E_{adj}—adjusted erosion rate; E_{rel}—relict erosion rate.

prior to ca. 10 Ma. The overlapping ranges of incision timings along the Clearwater River can be much lower (i.e., more recent) than those along the Salmon, but many 50 km sections have overlapping ranges of incision timings at or prior to ca. 5 Ma (Figs. 9A–9D).

These findings are supported by results using reference concavities of 0.3, 0.5, and 0.7, even when *tolerance* is fixed at 30 m (Fig. 9; Figs. S11 and S12) or individually calculated for each tributary (Figs. S13–S15). In each combination of *m*/*n* and *tolerance*, more tributaries have acceptable models for lower *n* values and the overlapping ranges of incision timings along the Salmon and Clearwater rivers precede ca. 10 Ma and ca. 5 Ma, respectively.

Comparison of the Incision Modeling Approaches

We used two different incision modeling approaches here (Table 2), and these approaches differ in their results, advantages, and disadvantages. The first approach (dividing incision depths by incision rates; Figs. 6 and 7) is simple and conceptually appealing, but it assumes that our estimated incision depths are accurate and does not provide an upper bound on incision timing (with the erosion rates used here; Fig. 5). Our second approach (finding best-fit model times; Figs. 8 and 9) does not rely on strict assumptions regarding initial conditions, lends itself to thoroughly exploring the parameter space in a manner that recognizes the uncertainties involved, and provides insight into the correlation between erodibility and rock type (Fig. 10). Despite these advantages, the vast number of potential incision timings produced by our second approach are less amenable to clear interpretation. Overall, we present both sets of incision timing estimates because their opposing advantages and disadvantages complement each other well. Furthermore,

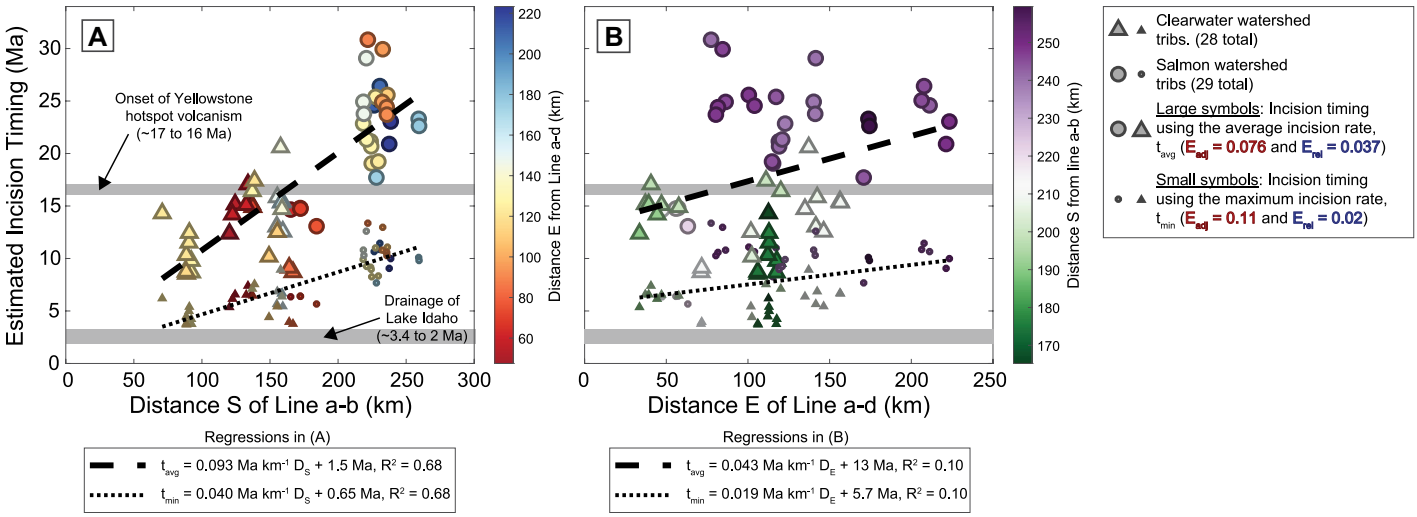

Figure 7. Estimated incision timings in the Salmon and Clearwater watersheds (Idaho, USA) shown by (A) each tributary's (tribs.) distance south of line a-b (D_S) and (B) each tributary's distance east of line a-d (D_E; Fig. 4A). E_{adj}—adjusted erosion rate; E_{rel}—relict erosion rate; t_{avg}—average time; t_{min}—minimum time.

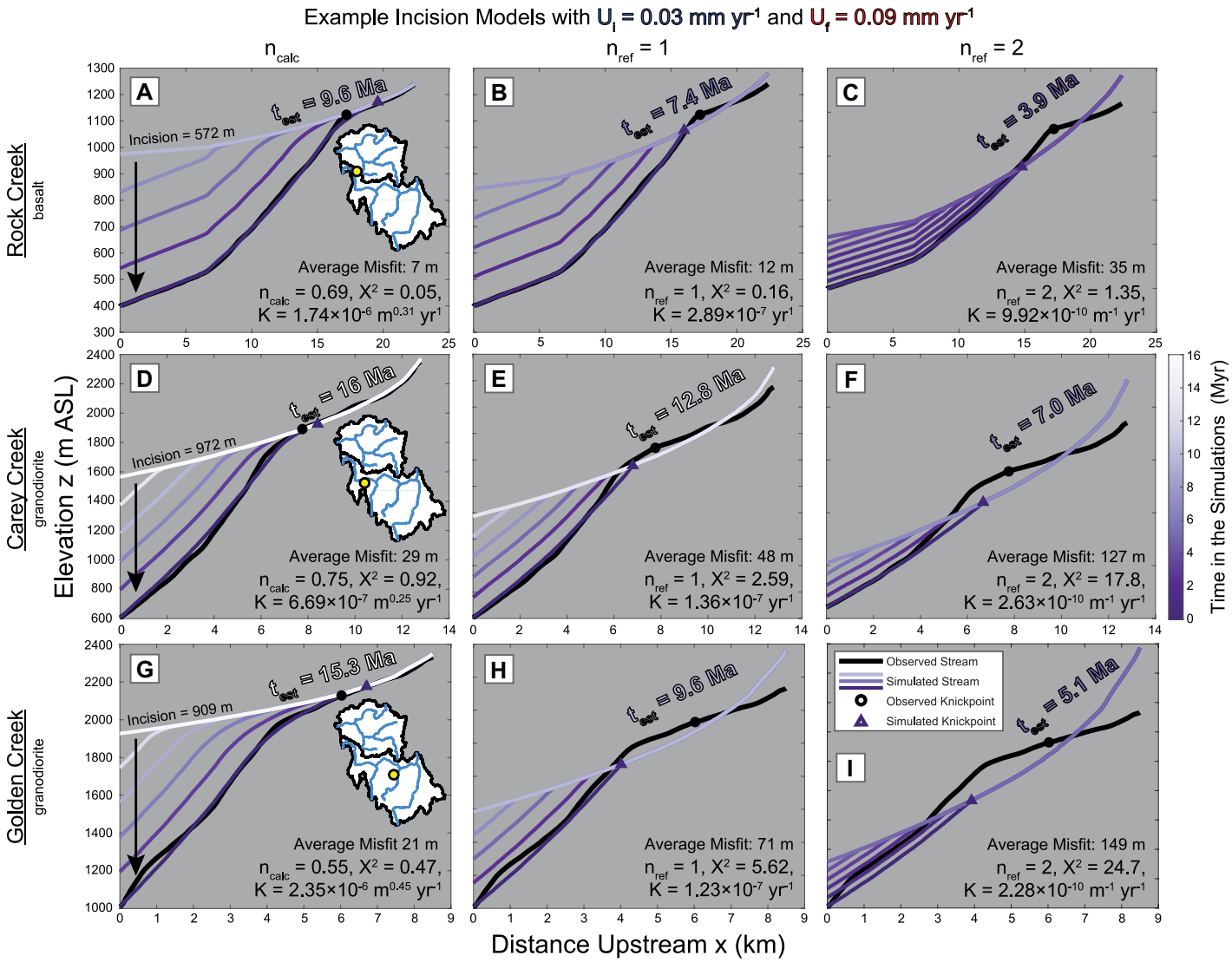

Figure 8. Examples of bedrock river incision models for three tributaries within the Salmon watershed (Idaho, USA). Subplots A–C show simulations for Rock Creek, subplots D–F show simulations for Carey Creek, and subplots G–I show simulations for Golden Creek. The final timestep in each subplot of Figure 8 is the best-fit model for that combination of model parameters (U_i—initial rock-uplift rate; U_f—final rock uplift rate; n—slope exponent; m—drainage area exponent), that tributary profile, and any time (t) between 0 and 34 m.y. The projected relict profiles were then found by evaluating the best-fit model's parameters at t = 0 years. Because of this distinction, the incision depths suggested by the projected relict profiles here are not always accurate (especially for the poor model fits using n_{ref} = 2 [n_{ref}—reference slope exponent n]). Note that this method for creating relict profiles is different than creating relict profiles from steepness regressions applied to the transient stream profiles, as shown in Figure 3. m ASL—meters above sea level; t_{est}—estimated time; n_{calc}—calculated slope exponent n.

both approaches suggest that transient incision began at ca. 5 and 10 Ma or earlier along the Clearwater and Salmon rivers, respectively, and we emphasize this point as our primary finding.

DISCUSSION

Taken together, our results indicate transient incision began along the Salmon River at ca. 10 Ma or earlier and along the Clearwater River farther to the north at ca. 5 Ma or earlier (Figs. 6–9). These incision timings predate the drainage of Lake Idaho (3.4–2 Ma; Staisch et al., 2022) and align more closely with the onset of the Yellowstone hotspot near southeastern Oregon at ca. 17–16 Ma (Pierce and Morgan, 1992, 2009). We interpret these results to mean that canyon incision in central Idaho was not initiated by the drainage of Lake Idaho, although the drainage could have accentuated the magnitude of incision. Below, we discuss the implications of these results with respect to the landscape evolution of the northern U.S. Cordillera as well as the role of lithology in the parameterization of bedrock river incision models.

Landscape Evolution of the Northern U.S. Cordillera

Our results show that transient incision in the Salmon and Clearwater watersheds has been ongoing for a relatively long duration. Indeed, even when thoroughly exploring the parameter

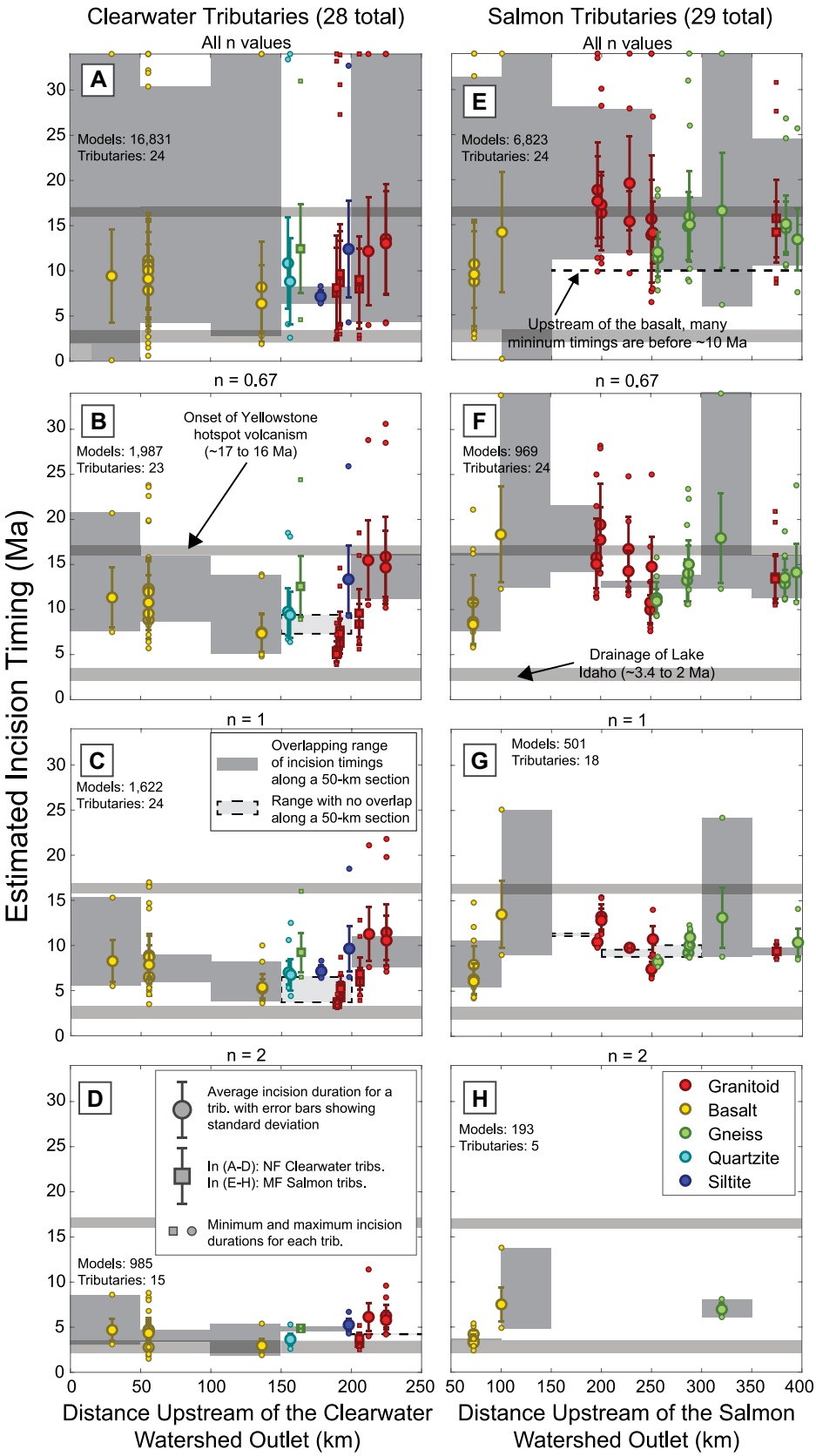

Figure 9. Incision timings from all acceptable models ($X^2 \leq 1$) for tributaries (Tribs) in (A–D) the Clearwater watershed and (E–H) the Salmon watershed (Idaho, USA). In four instances, a 50 km section did not have an overlapping range of incision timings; in that 50 km section, the highest minimum acceptable timing is above the lowest maximum acceptable timing. In such cases, the highlighted range represents the corresponding separation between highest minimum and lowest maximum incision timing. Incision timings for tributaries along the North Fork Clearwater and Middle Fork Salmon rivers (Fig. 1A) are shown as squares because those tributaries are situated farther from the other tributaries shown. Note that that these rivers are included in the overlapping ranges of timings in several 50 km sections (150–250 km in A–D and 350–400 km in E–H). Even with the selection criteria used here (e.g., carefully inspecting stream profile data and only selecting tributaries underlain by one rock type), four tributaries to the Clearwater River and five tributaries to the Salmon River never received any acceptable models. NF—North Fork; MF—Middle Fork.

space of the stream power model our results along the Salmon River suggest canyon incision began no later than ca. 10 Ma, during the mid- to late Miocene or earlier (Figs. 6B and 9E). Along the deeply incised portion of the Salmon River (upstream of the basalt), our results show the Salmon River canyon could be as old as ca. 25 or 30 Ma (Figs. 6B and 9E). We emphasize, however, that we are more confident in the lower boundary of 10 Ma than any specific upper boundary. Nonetheless, these potential incision timings imply that a variety of early (ca. 30–10 Ma) events may be related to canyon incision in central Idaho. Such events include (Table 1) lava damming by CRB flows (Camp, 1981; Camp et al., 1982; Larimer et al., 2019), subsidence within the Columbia Basin (Reidel et al., 1989, 2013; Reidel and Tolan, 2013; Perry-Houts and Humphreys, 2018), the reactivation of the Salmon River suture zone following CRB eruptions (Tikoff et al., 2001), the extensional collapse of a crustal plateau (Byerly et al., 2017; Fayon et al., 2017; Kahn et al., 2020), and uplift from flexure and/or lower crustal flow (McQuarrie and Rodgers, 1998; Yuan et al., 2010). Furthermore, these events generally have a connection to the Yellowstone hotspot. For example, the hotspot is thought to have caused CRB extrusions (Hooper et al.,

2007; Camp and Hanan, 2008) and acted as a catalyst for Basin and Range extension (Parsons et al., 1994; Camp et al., 2015, although this relationship is debated; Colgan et al., 2004). The timing of factors like lava damming and the reactivation of the Salmon River suture zone are thus aligned with the timing of the hotspot's passage through southern Idaho. Such interconnections make it difficult to isolate the influence of each individual potential driver of canyon incision. We do not identify any specific event as the main driver of canyon incision, but instead argue that canyon incision was driven by a combination of factors related to the Yellowstone hotspot. Canyon incision in central Idaho reflects processes that have been ongoing for ≥10 m.y., highlighting the potential for landscape morphology to record geological history.

The timing of incision along basalt tributaries might be further constrained through the combination of incision timing estimates and basalt geochronology. The lowest minimum incision timing from Equation 6 for these basalt tributaries is 5.4 Ma (Fig. 6). As discussed in the background section, basalt tributaries have incised through CRB flows as young as ca. 11.5 Ma (Fig. 2B). Our results could therefore suggest that transient incision along the Salmon and Clearwater rivers in this vicinity began between ca. 11.5 and 5.4 Ma. One should note, however, that this age constraint does not include the time required for drainage network development within the basalt. For example, drainage network development within basalt of the Cascade Range of central Oregon required over 1 m.y. (Jefferson et al., 2010). Before these basalt tributaries could respond to canyon incision along the Salmon and Clearwater rivers, they first had to develop integrated channel networks. This uncertainty is compounded by the fact that we lack relict and adjusted erosion rates within the basalt (Fig. 2A). Furthermore, it is possible that the extrusion of basalts occurred during regional incision; if so, basalt flow ages would not provide an upper limit for incision timing throughout the region. Nonetheless, results for nearby tributaries in locations where we do have cosmogenic erosion rates (e.g., along the Middle Fork Clearwater and Lochsa rivers; Figs. 1A and 2A) also suggest that transient incision has been ongoing since ca. 5 Ma (Fig. 6A). We therefore estimate that the transient incision of these basalt tributaries began between ca. 11.5 and ca. 5 Ma.

The contrasting incision depths (Fig. 3) and incision timing estimates (Figs. 6 and 9) along the Salmon and Clearwater rivers could indicate spatial differences in the timing of canyon incision in central Idaho. In the south, canyon incision along the Salmon River initiated at ca. 10 Ma or earlier, whereas canyon incision along the Clearwater River in the north may have begun more recently at ca. 5 Ma or earlier. Although our cosmogenic erosion rates do not suggest an increase in erosion rates to the south (Fig. 5A), canyon incision may have begun earlier at locations closer to the Yellowstone hotspot track. Indeed, such conditions could correspond with the northwards surface tilting proposed by Larimer et al. (2019). In the case of surface uplift due to lower crustal flow (McQuarrie and Rodgers, 1998; Yuan et al., 2010), the north-to-south increase in both incision depths (Fig. 1A) and estimated incision timings (Fig. 7A) could reflect the intensity and spatiotemporal evolution of lower crustal flow away from the eastern Snake River Plain. Otherwise, faulting and the extensional collapse of a crustal plateau (Tikoff et al., 2001; Byerly et al., 2017; Fayon et al., 2017; Kahn et al., 2020) or the subsidence of areas with extensive CRB flows (Reidel et al., 1989, 2013; Reidel and Tolan, 2013; Perry-Houts and Humphreys, 2018) may have influenced the Salmon and Clearwater watersheds in different ways, potentially allowing for the earlier creation of the Salmon River canyon. However, it is difficult to imagine a scenario that initiates transience along the Salmon River 5 m.y. before the Clearwater River. Our results could allow for canyon incision starting at ca. 10 Ma in both watersheds (Figs. 6 and 9). That timing would be close to the minimum incision timing from Equation 6 in the Salmon watershed (Fig. 6B) but greater than the minimum incision timing in the Clearwater watershed (Fig. 6A), an arrangement that would imply spatially variable erosion rates (e.g., higher adjusted erosion rates along the Salmon). Our cosmogenic erosion rates (Figs. 4 and 5) do not clearly demonstrate such systematic changes in erosion rate over space.

We acknowledge that the methods we employ have limitations. For example, cosmogenic erosion rates involve considerable uncertainties and they are representative over limited timescales (Bierman, 1994). We therefore cannot assert definitively that erosion rates have been sustained over time as bimodal relict and adjusted erosion rates of ∼0.037 and 0.076 mm yr^{-1} (Fig. 5). These erosion rates are relatively similar to the cooling rates from thermochronology data available for the region, however, with $^{40}Ar/^{39}Ar$ cooling ages showing exhumation rates of 0.05–0.06 mm yr^{-1} since 78 Ma near Elk City, Idaho (Fig. 1A; Lund et al., 1986), and fission-track data showing exhumation rates of 0.03–0.1 mm yr^{-1} since 50 Ma in the Boise Mountains (Fig. 1A; Sweetkind and Blackwell, 1989). Although one might estimate erosion rates over time with inversion approaches for the stream power model (Goren et al., 2014), the choices commonly used in such approaches (e.g., assuming $n = 1$) would be particularly problematic in this landscape. We discuss such considerations in the section below. We have focused on modeling a step change in erosion rates because (1) our cosmogenic erosion rates from the high- and low-relief portions of central Idaho generally demonstrate variations around mean values (Fig. 5), (2) it is a conceptually simple starting point for unraveling the history of this landscape, (3) the consistent presence of high- and low-steepness reaches along transient tributaries (Fig. 3) makes this approach work well within the framework of the stream power model, and (4) without more constraints on erosion rate variations over time, the potential variations are limitless (both over time and across these large watersheds). If base level fall rates in the past were considerably higher than our adjusted erosion rates, then these rates may have been short-lived. Otherwise, these rates would likely be more imprinted over a larger proportion of the modern landscape (Willenbring et al., 2013). Such considerations and many others inherent within river incision modeling (e.g., the roles of sediment cover, large boulders, and discharge variability; Sklar and Dietrich, 2001; DiBiase and Whipple, 2011; Glade et al., 2019) imply that a more detailed accounting of the landscape evolution of central Idaho will require further study. Regardless, if events and processes related to the Yellowstone hotspot have contributed to canyon incision in central Idaho, as hypothesized here, then this relationship would highlight the role of deep lithosphere/mantle processes on the landscape evolution of the northern U.S. Cordillera. The interaction between a mantle plume and continental lithosphere could lead to unique scenarios of landscape evolution, and the canyon incision in central Idaho may be an example of such interactions.

Lithology and River Incision Model Parameterization

The river incision models we use to constrain incision timing also demonstrate a relationship between rock type and bedrock erodibility. Indeed, our model results show a contrast in erodibility between basalt and the other lithologies within the study area (Fig. 10). For the sake of concision, we only show erodibilities for three n values: $n = 0.67$ (Fig. 10A), $n = 1$ (Fig. 10B), and $n = 1.5$ (Fig. 10C). Nonetheless, the trend apparent in Figure 10 is consistent across different n values. Regardless of the n value used, the erodibilities for basalt tributaries are generally higher than those for tributaries underlain by the other rock types assessed here (granitoid,

gneiss, quartzite, and siltite). The other rock types generally have acceptable models with similar erodibilities. Even though basalt can have a relatively high tensile strength (Sklar and Dietrich, 2001; Bursztyn et al., 2015), our field surveys indicate these basalt flows often feature extensive fractures (e.g., joints within columnar basalts) that likely reduce the basalt's rock mass strength and increase its susceptibility to fluvial erosion. Additionally, basalt mineralogy is highly susceptible to chemical weathering which may feedback into erosion processes (Murphy et al., 2016). One should note, however, that basalt does not yield quartz and we do not have any erosion rates within basalt watersheds. As a result, the relict erosion rates in basalt drainage basins could be lower than our relict erosion rates, which would impact the erodibilities estimated through incision modeling. The wide range of erosion rates used in our incision models (Table 2) does include erosion rates as low as about half of the average relict erosion rate, however (0.02 mm yr^{-1} versus the average relict erosion rate of ~0.037 mm yr^{-1}).

The erodibility contrast between basalt and the other rock types (Fig. 10) varies with the reference concavity used. For $\theta_{ref} = 0.3$, acceptable model fits suggest that basalt tributaries have even higher erodibilities relative to tributaries from other rock types (Figs. S16 and S19). For $\theta_{ref} = 0.7$, however, the erodibility contrast between basalt and the other rock types disappears; acceptable model fits using $\theta_{ref} = 0.7$ generally suggest all rock types have similar erodibilities (Figs. S17 and S20). These distinctions reflect the sensitivity of erosion rate to drainage area (Equation 1); with $\theta_{ref} = 0.7$, the faster rate of channel slope reduction with drainage area (Equation 2) could make incision models less sensitive to variations in erodibility. Conversely, the reduced sensitivity of channel slope to drainage area when $\theta_{ref} = 0.3$ could make incision models more sensitive to variations in erodibility.

We optimized erodibility in our incision models, but changes in erodibility through optimization were relatively small (Figs. S21–S26). In other words, there was generally a small contrast between the K initially calculated with Equation 9 and the final best-fit erodibility after assessing many different K values. For example, the K values in Figure 10 are generally within 5% and always within 15.5% of the K from Equation 9. Even though the K from Equation 9 is only based on a measured adjusted steepness and assumed n and U values, the best-fit K found through incision modeling reflects a wider range of factors like the relict steepness and the shape of the knickzone (which reflects K, n, m, and changes in drainage area along the profile). These results therefore support the utility of Equation 9 for calculating erodibility.

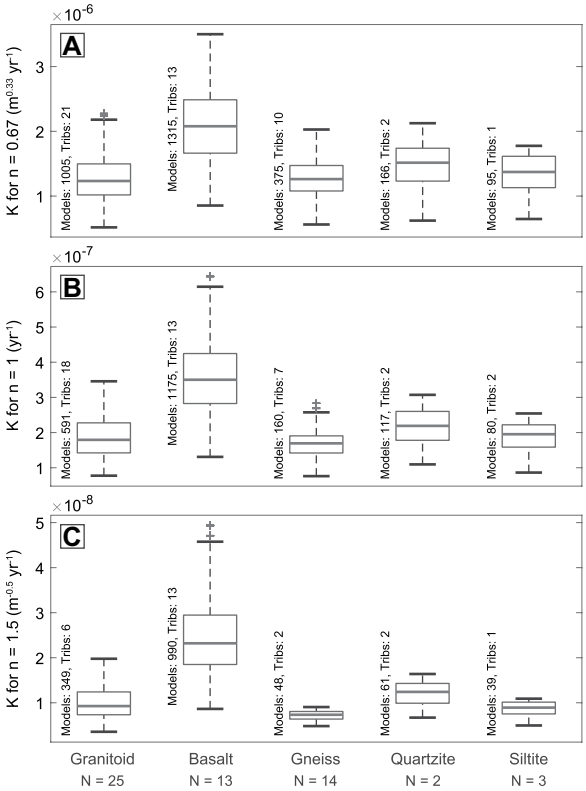

Figure 10. Erodibility (K) values for all acceptable models ($X2 \leq 1$) using (A) n = 0.67, (B) n = 1, and (C) n = 1.5. Next to each distribution, we show the number of stream profiles ("Tribs") underlain by that rock type with acceptable models as well as the number of acceptable models. The total number of stream profiles for each rock type is shown as N at the bottom.

We observe variations in transient stream morphology that could represent a dependence of slope exponent n on rock type. Basalt tributaries in our study area tend to have discrete knickpoints located at an abrupt change in steepness (Figs. 3B and 8A). In the context of the stream power model, such transient morphologies are produced for $n \geq 1$ (Royden and Perron, 2013; Mitchell and Yanites, 2019). Conversely, transient streams in the other rock types we study (granitoid, gneiss, quartzite, and siltite) generally have convex knickzones separating relict and adjusted reaches (Figs. 3A, 3C, and 8B). Such morphologies are produced by stream power models using $n < 1$ (Royden and Perron, 2013; Mitchell and Yanites, 2019). Variations in n with rock type could reflect dominant incision processes, and Whipple et al. (2000a) proposed that abrasion by suspended sediment should correspond with an n value of ~5/3 while plucking should correspond with n values of 2/3 to 1. Indeed, if n partially reflects the effects of sediment abrasion, it may also reflect the influence of lithology on the strength and grain size distributions of sediment yielded from hillslopes to channels (Sklar and Dietrich, 2001; Sklar et al., 2017; Roda-Boluda et al., 2018). Slope exponent n may also reflect hydraulic geometries and runoff variability (Lague et al., 2005; Lague, 2014), with lower n values corresponding with greater runoff variability. Tributaries in each rock type received acceptable models using a range of reference n values (Figs. 8 and 9; Figs. S27 and S28) and calculated n values (n_{calc} ranged from 0.040 to 2.47; Figs. S29 and S30), but only models using $n \geq 1$ can produce the sharp knickpoints consistently present in basalt tributaries. We do not have proof of a covariation between rock type and slope exponent n, but if this covariation occurs it could have (1) a significant impact on the spatiotemporal evolution of transient incision in central Idaho and (2) significant implications for modeling landscapes with variable lithology. Overall, the sensitivity of our model results to slope exponent n values (Figs. 8 and 9) highlights that sweeping assumptions regarding n (e.g., always assuming $n = 1$) can significantly impact model predictions.

CONCLUSIONS

In this study, we have shown that transient incision along the Salmon River of Idaho likely began at ca. 10 Ma or earlier while transient incision along the Clearwater River farther to the north likely began at ca. 5 Ma or earlier (Figs. 6–9). Based on the ages of basalt flows underlying tributaries to these rivers, we estimate the incision of these basalt tributaries began between ca. 11.5 and 5 Ma. These spa-

tial variations in estimated incision timings could indicate earlier canyon incision to the south, potentially reflecting surface uplift that has propagated northwards over time. Based on both the timing and spatial patterns, we argue that canyon incision in these watersheds is driven by events and processes related to the Yellowstone hotspot. Such events include lava damming from Columbia River Basalt (CRB) flows (Camp, 1981; Camp et al., 1982; Larimer et al., 2019), subsidence in the Columbia Basin during CRB extrusions (Reidel et al., 1989, 2013; Reidel and Tolan, 2013; Perry-Houts and Humphreys, 2018), faulting along the Salmon River suture zone after CRB extrusions (Tikoff et al., 2001), and potential surface uplift from lower crustal flow (McQuarrie and Rodgers, 1998; Yuan et al., 2010). We demonstrate these findings by compiling a collection of 46 cosmogenic erosion rates (17 of which are new) from in situ ^{10}Be concentrations in fluvial sediment and estimating the incision timings of 57 stream profiles within the Salmon and Clearwater watersheds using bedrock river incision models. Our cosmogenic erosion rates targeted both the low-relief and high-relief portions of central Idaho, which we interpret to be relict and adjusted landscapes, respectively. Relict erosion rates varied around an average of 0.037 mm yr^{-1}, while adjusted erosion rates varied around an average of 0.076 mm yr^{-1}. These data imply roughly a doubling in base level fall rates, with no clear spatial signature shown in the variation of either relict or adjusted erosion rates. We also modeled the incision histories of transient river profiles. Our model results highlight how assumptions regarding slope exponent n (i.e., always assuming $n = 1$) can significantly impact model results. Regardless of the n value used, our models suggest basalt could be more erodible than the other rock types we focus on (granitoids, gneiss, quartzite, and siltite) despite the high tensile strength of basalt (Sklar and Dietrich, 2001; Bursztyn et al., 2015). These findings highlight the complicated role of lithology in fluvial erosion and landscape transience. Our findings highlight how the interaction between a mantle plume and continental lithosphere could have dramatic implications for landscape evolution. Central Idaho may therefore be an exemplary illustration of the interactions between geodynamics and surface processes.

ACKNOWLEDGMENTS

This work was supported by (1) grants from the National Science Foundation (NSF-EAR grants 1727139 and 1727046), (2) a scholarship from the Tobacco Root Geological Society, and (3) the Thornbury Fellowship at Indiana University's Department of Earth and Atmospheric Sciences. This research was supported in part by Lilly Endowment, Inc., through its support for the Indiana University Pervasive Technology Institute. This study's data are available in the IUScholarWorks Data Repository at Indiana University (http://hdl.handle.net/2022/26678).

REFERENCES CITED

Adams, B.A., Whipple, K.X., Forte, A.M., Heimsath, A.M., and Hodges, K.V., 2020, Climate controls on erosion in tectonically active landscapes: Science Advances, v. 6, https://doi.org/10.1126/sciadv.aaz3166.

Allen, G.H., Barnes, J.B., Pavelsky, T.M., and Kirby, E., 2013, Lithologic and tectonic controls on bedrock channel form at the northwest Himalayan front: Journal of Geophysical Research: Earth Surface, v. 118, p. 1806–1825, https://doi.org/10.1002/jgrf.20113.

Armstrong, I.P., Yanites, B.J., Mitchell, N., DeLisle, C., and Douglas, B.J., 2021, Quantifying normal fault evolution from river profile analysis in the northern Basin and Range Province, southwest Montana, USA: Lithosphere, v. 2021, no. 1, https://doi.org/10.2113/2021/7866219.

Barry, T.L., Kelley, S.P., Reidel, S.P., Camp, V.E., Self, S., Jarboe, N.A., Duncan, R.A., and Renne, P.R., 2013, Eruption chronology of the Columbia River Basalt Group, *in* Reidel, S.P., Camp, V.E., Ross, M.E., Wolff, J.A., Martin, B.S., Tolan, T.C., and Wells, R.E., eds., The Columbia River Flood Basalt Province: Geological Society of America Special Paper 497, p. 45–66, https://doi.org/10.1130/2013.2497(02).

Beranek, L.P., Link, P.K., and Fanning, C.M., 2006, Miocene to Holocene landscape evolution of the western Snake River Plain region, Idaho: Using the SHRIMP detrital zircon provenance record to track eastward migration of the Yellowstone hotspot: Geological Society of America Bulletin, v. 118, p. 1027–1050, https://doi.org/10.1130/B25896.1.

Berlin, M.M., and Anderson, R.S., 2007, Modeling of knickpoint retreat on the Roan Plateau, western Colorado: Journal of Geophysical Research: Earth Surface, v. 112, https://doi.org/10.1029/2006JF000553.

Bierman, P., and Steig, E.J., 1996, Estimating rates of denudation using cosmogenic isotope abundance in sediment: Earth Surface Processes and Landforms, v. 21, n. 2, p. 125-139, https://doi.org/10.1002/(SICI)1096-9837(199602)21:2<125::AID-ESP511>3.0.CO;2-8.

Bierman, P.R., 1994, Using in situ produced cosmogenic isotopes to estimate rates of landscape evolution: A review from the geomorphic perspective: Journal of Geophysical Research: Solid Earth, v. 99, p. 13,885–13,896, https://doi.org/10.1029/94JB00459.

Blackwelder, E., 1912, The old erosion surface in Idaho: A criticism: The Journal of Geology, v. 20, p. 410–414, https://doi.org/10.1086/621986.

Braucher, R., Del Castillo, P., Siame, L., Hidy, A.J., and Bourlés, D.L., 2009, Determination of both exposure time and denudation rate from an in situ-produced ^{10}Be depth profile: A mathematical proof of uniqueness. Model sensitivity and applications to natural cases: Quaternary Geochronology, v. 4, p. 56–67, https://doi.org/10.1016/j.quageo.2008.06.001.

Brown, E.T., Brook, E.J., Raisbeck, G.M., Yiou, F., and Kurz, M.D., 1992, Effective attenuation lengths of cosmic rays producing ^{10}Be AND ^{26}Al in quartz: Implications for exposure age dating: Geophysical Research Letters, v. 19, p. 369–372, https://doi.org/10.1029/92GL00266.

Bursztyn, N., Pederson, J.L., Tressler, C., Mackley, R.D., and Mitchell, K.J., 2015, Rock strength along a fluvial transect of the Colorado Plateau: Quantifying a fundamental control on geomorphology: Earth and Planetary Science Letters, v. 429, p. 90–100, https://doi.org/10.1016/j.epsl.2015.07.042.

Byerly, A., Tikoff, B., Kahn, M., Jicha, B., Gaschnig, R., and Fayon, A.K., 2017, Internal fabrics of the Idaho batholith, USA: Lithosphere, v. 9, p. 283–298, https://doi.org/10.1130/L551.1.

Camp, V.E., 1981, Geologic studies of the Columbia Plateau: Part II. Upper Miocene basalt distribution, reflecting source locations, tectonism, and drainage history in the Clearwater embayment, Idaho: Geological Society of America Bulletin, v. 92, p. 669–678, https://doi.org/10.1130/0016-7606(1981)92<669:GSOTCP>2.0.CO;2.

Camp, V.E., 1995, Mid-Miocene propagation of the Yellowstone mantle plume head beneath the Columbia River basalt source region: Geology, v. 23, p. 435, https://doi.org/10.1130/0091-7613(1995)023<0435:MMPOTY>2.3.CO;2.

Camp, V.E., and Hanan, B.B., 2008, A plume-triggered delamination origin for the Columbia River Basalt Group: Geosphere, v. 4, p. 480–495, https://doi.org/10.1130/GES00175.1.

Camp, V.E., Hooper, P.R., Swanson, A., and Wright, T.L., 1982, The Columbia River Basalt in Idaho: Physical and chemical characteristics, flow distribution, and tectonic implications, *in* Bonnichsen, B., Breckenridge, R.M., eds., Cenozoic Geology of Idaho: Idaho Bureau of Mines and Geology Bulletin, v. 26, p. 55–75.

Camp, V.E., Pierce, K.L., and Morgan, L.A., 2015, Yellowstone plume trigger for Basin and Range extension, and coeval emplacement of the Nevada–Columbia Basin magmatic belt: Geosphere, v. 11, p. 203–225, https://doi.org/10.1130/GES01051.1.

Codilean, A.T., 2006, Calculation of the cosmogenic nuclide production topographic shielding scaling factor for large areas using DEMs: Earth Surface Processes and Landforms, v. 31, p. 785–794, https://doi.org/10.1002/esp.1336.

Colgan, J.P., Dumitru, T.A., and Miller, E.L., 2004, Diachroneity of Basin and Range extension and Yellowstone hotspot volcanism in northwestern Nevada: Geology, v. 32, p. 121, https://doi.org/10.1130/G20037.1.

Coulthard, T.J., and Van De Wiel, M.J., 2012, Modelling river history and evolution: Philosophical Transactions of the Royal Society A. Mathematical, Physical and Engineering Sciences, v. 370, p. 2123–2142, https://doi.org/10.1098/rsta.2011.0597.

Crosby, B.T., and Whipple, K.X., 2006, Knickpoint initiation and distribution within fluvial networks: 236 waterfalls in the Waipaoa River, North Island, New Zealand: Geomorphology, v. 82, p. 16–38, https://doi.org/10.1016/j.geomorph.2005.08.023.

Crow, R., Karlstrom, K., Darling, A., Crossey, L., Polyak, V., Granger, D., Asmerom, Y., and Schmandt, B., 2014, Steady incision of Grand Canyon at the million year timeframe: A case for mantle-driven differential uplift: Earth and Planetary Science Letters, v. 397, p. 159–173, https://doi.org/10.1016/j.epsl.2014.04.020.

Darold, A., and Humphreys, E., 2013, Upper mantle seismic structure beneath the Pacific Northwest: A plume-triggered delamination origin for the Columbia River flood basalt eruptions: Earth and Planetary Science Letters, v. 365, p. 232–242, https://doi.org/10.1016/j.epsl.2013.01.024.

DiBiase, R.A., 2018, Short communication: Increasing vertical attenuation length of cosmogenic nuclide production on steep slopes negates topographic shielding corrections for catchment erosion rates: Earth Surface Dynamics, v. 6, p. 923–931, https://doi.org/10.5194/esurf-6-923-2018.

DiBiase, R.A., and Whipple, K.X., 2011, The influence of erosion thresholds and runoff variability on the relationships among topography, climate, and erosion rate: Journal of Geophysical Research: Earth Surface, v. 116, F4, https://doi.org/10.1029/2011JF002095.

DiBiase, R.A., Rossi, M.W., and Neely, A.B., 2018, Fracture density and grain size controls on the relief structure of bedrock landscapes: Geology, v. 46, p. 399–402, https://doi.org/10.1130/G40006.1.

Dickinson, W.R., 2004, Evolution of the North American Cordillera: Annual Review of Earth and Planetary Sciences, v. 32, p. 13–45, https://doi.org/10.1146/annurev.earth.32.101802.120257.

Dodson, A., Kennedy, B.M., and DePaolo, D.J., 1997, Helium and neon isotopes in the Imnaha Basalt, Columbia River Basalt Group: Evidence for a Yellowstone plume source: Earth and Planetary Science Letters, v. 150, p. 443–451, https://doi.org/10.1016/S0012-821X(97)00090-3.

Duvall, A., Kirby, E., and Burbank, D., 2004, Tectonic and lithologic controls on bedrock channel profiles and processes in coastal California: Journal of Geophysical Research: Earth Surface, v. 109, F3, https://doi.org/10.1029/2003JF000086.

Duvall, A.R., Harbert, S.A., Upton, P., Tucker, G.E., Flowers, R.M., and Collett, C., 2020, River patterns reveal two stages of landscape evolution at an oblique convergent margin, Marlborough Fault System, New Zealand: Earth Surface Dynamics, v. 8, p. 177–194, https://doi.org/10.5194/esurf-8-177-2020.

Elkins-Tanton, L.T., 2007, Continental magmatism, volatile recycling, and a heterogeneous mantle caused by lithospheric gravitational instabilities: Journal of Geophysical Research: Solid Earth, v. 112, B3, https://doi.org/10.1029/2005JB004072.

Ellis, M.A., Barnes, J.B., and Colgan, J.P., 2015, Geomorphic evidence for enhanced Pliocene–Quaternary faulting in the northwestern Basin and Range: Lithosphere, v. 7, p. 59–72, https://doi.org/10.1130/L401.1.

Fayon, A.K., Tikoff, B., Kahn, M., and Gaschnig, R.M., 2017, Cooling and exhumation of the southern Idaho batholith: Lithosphere, v. 9, p. 299–314, https://doi.org/10.1130/L565.1.

Flowers, R.M., Wernicke, B.P., and Farley, K.A., 2008, Unroofing, incision, and uplift history of the southwestern Colorado Plateau from apatite (U-Th)/He thermochronometry: Geological Society of America Bulletin, v. 120, p. 571–587, https://doi.org/10.1130/B26231.1.

Foster, D.A., Schafer, C., Fanning, C.M., and Hyndman, D.W., 2001, Relationships between crustal partial melting, plutonism, orogeny, and exhumation: Idaho–Bitterroot batholith: Tectonophysics, v. 342, p. 313–350, https://doi.org/10.1016/S0040-1951(01)00169-X.

Gallen, S.F., and Fernández-Blanco, D., 2021, A new data-driven Bayesian inversion of fluvial topography clarifies the tectonic history of the Corinth Rift and reveals a channel steepness threshold: Journal of Geophysical Research: Earth Surface, v. 126, no. 3, https://doi.org/10.1029/2020JF005651.

Gallen, S.F., and Wegmann, K.W., 2017, River profile response to normal fault growth and linkage: An example from the Hellenic forearc of south-central Crete, Greece: Earth Surface Dynamics, v. 5, p. 161–186, https://doi.org/10.5194/esurf-5-161-2017.

Gallen, S.F., Wegmann, K.W., Frankel, K.L., Hughes, S., Lewis, R.Q., Lyons, N., Paris, P., Ross, K., Bauer, J.B., and Witt, A.C., 2011, Hillslope response to knickpoint migration in the Southern Appalachians: Implications for the evolution of post-orogenic landscapes: Earth Surface Processes and Landforms, v. 36, p. 1254–1267, https://doi.org/10.1002/esp.2150.

Gaschnig, R.M., Vervoort, J.D., Lewis, R.S., and Tikoff, B., 2011, Isotopic evolution of the Idaho Batholith and Challis Intrusive Province, northern US Cordillera: Journal of Petrology, v. 52, p. 2397–2429, https://doi.org/10.1093/petrology/egr050.

Glade, R.C., Shobe, C.M., Anderson, R.S., and Tucker, G.E., 2019, Canyon shape and erosion dynamics governed by channel-hillslope feedbacks: Geology, v. 47, p. 650–654, https://doi.org/10.1130/G46219.1.

Goode, J.R., and Wohl, E., 2010, Substrate controls on the longitudinal profile of bedrock channels: Implications for reach-scale roughness: Journal of Geophysical Research: Earth Surface, v. 115, F3, https://doi.org/10.1029/2008JF001188.

Goren, L., Fox, M., and Willett, S.D., 2014, Tectonics from fluvial topography using formal linear inversion: Theory and applications to the Inyo Mountains, California: Journal of Geophysical Research: Earth Surface, v. 119, p. 1651–1681, https://doi.org/10.1002/2014JF003079.

Gosse, J.C., and Phillips, F.M., 2001, Terrestrial in situ cosmogenic nuclides: Theory and application: Quaternary Science Reviews, v. 20, p. 1475–1560, https://doi.org/10.1016/S0277-3791(00)00171-2.

Gran, K.B., Finnegan, N., Johnson, A.L., Belmont, P., Wittkop, C., and Rittenour, T., 2013, Landscape evolution, valley excavation, and terrace development following abrupt postglacial base-level fall: Geological Society of America Bulletin, v. 125, p. 1851–1864, https://doi.org/10.1130/B30772.1.

Granger, D.E., Kirchner, J.W., and Finkel, R., 1996, Spatially averaged long-term erosion rates measured from in situ-produced cosmogenic nuclides in alluvial sediment: The Journal of Geology, v. 104, p. 249–257, https://doi.org/10.1086/629823.

Hamilton, W.B., 1963, Metamorphism in the Riggins region, western Idaho: U.S. Geological Survey Professional Paper 436, 95 p., https://doi.org/10.3133/pp436.

Harel, M.-A., Mudd, S.M., and Attal, M., 2016, Global analysis of the stream power law parameters based on worldwide ^{10}Be denudation rates: Geomorphology, v. 268, p. 184–196, https://doi.org/10.1016/j.geomorph.2016.05.035.

Harkins, N., Kirby, E., Heimsath, A., Robinson, R., and Reiser, U., 2007, Transient fluvial incision in the headwaters of the Yellow River, northeastern Tibet, China: Journal of Geophysical Research: Earth Surface, v. 112, https://doi.org/10.1029/2006JF000570.

Hooper, P.R., Camp, V.E., Reidel, S.P., and Ross, M.E., 2007, The origin of the Columbia River flood basalt province: Plume versus nonplume models, *in* Plates, Plumes and Planetary Processes: Geological Society of America Special Paper 430, p. 635–668, https://doi.org/10.1130/2007.2430(30).

Howard, A.D., 1965, Geomorphological systems; equilibrium and dynamics: American Journal of Science, v. 263, p. 302–312, https://doi.org/10.2475/ajs.263.4.302.

Howard, A.D., 1994, A detachment-limited model of drainage basin evolution: Water Resources Research, v. 30, p. 2261–2285, https://doi.org/10.1029/94WR00757.

Howard, A.D., and Kerby, G., 1983, Channel changes in badlands: Geological Society of America Bulletin, v. 94, p. 739–752, https://doi.org/10.1130/0016-7606(1983)94<739:CCIB>2.0.CO;2.

Ibarra, D.E., Caves, J.K., Moon, S., Thomas, D.L., Hartmann, J., Chamberlain, C.P., and Maher, K., 2016, Differential weathering of basaltic and granitic catchments from concentration-discharge relationships: Geochimica et Cosmochimica Acta, v. 190, p. 265–293, https://doi.org/10.1016/j.gca.2016.07.006.

Janecke, S.U., 1992, Kinematics and timing of three superposed extensional systems, east central Idaho: Evidence for an Eocene tectonic transition: Tectonics, v. 11, p. 1121–1138, https://doi.org/10.1029/92TC00334.

Janecke, S.U., Geissman, J.W., and Bruhn, R.L., 1991, Localized rotation during Paleogene Extension in east central Idaho: Paleomagnetic and geologic evidence: Tectonics, v. 10, p. 403–432, https://doi.org/10.1029/90TC02465.

Janecke, S.U., VanDenburg, C.J., Blankenau, J.J., and M'Gonigle, J.W., 2000, Long-distance longitudinal transport of gravel across the Cordilleran thrust belt of Montana and Idaho: Geology, v. 28, p. 439–442, https://doi.org/10.1130/0091-7613(2000)28<439:LLTOGA>2.0.CO;2.

Jefferson, A., Grant, G.E., Lewis, S.L., and Lancaster, S.T., 2010, Coevolution of hydrology and topography on a basalt landscape in the Oregon Cascade Range, USA: Earth Surface Processes and Landforms, v. 35, no. 7, p. 803–816, https://doi.org/10.1002/esp.1976.

Jeffery, M.L., Ehlers, T.A., Yanites, B.J., and Poulsen, C.J., 2013, Quantifying the role of paleoclimate and Andean Plateau uplift on river incision: Journal of Geophysical Research: Earth Surface, v. 118, p. 852–871, https://doi.org/10.1002/jgrf.20055.

Kahn, M., Fayon, A.K., and Tikoff, B., 2020, Constraints on the post-orogenic tectonic history along the Salmon River suture zone from low-temperature thermochronology, western Idaho and eastern Oregon: Rocky Mountain Geology, v. 55, p. 27–54, https://doi.org/10.24872/rmgjournal.55.1.27.

Karlstrom, K.E., Crow, R., Crossey, L.J., Coblentz, D., and Van Wijk, J.W., 2008, Model for tectonically driven incision of the younger than 6 Ma Grand Canyon: Geology, v. 36, p. 835, https://doi.org/10.1130/G25032A.1.

Kasbohm, J., and Schoene, B., 2018, Rapid eruption of the Columbia River flood basalt and correlation with the mid-Miocene climate optimum: Science Advances, v. 4, no. 9, https://doi.org/10.1126/sciadv.aat8223.

Kauffman, J.D., Garwood, D.L., Schmidt, K.L., Lewis, R.S., Othberg, K.L., and Phillips, W.M., 2009, Geologic Map of the Idaho Parts of the Orofino and Clarkston 30 x 60 Minute Quadrangles, Idaho: Moscow, Idaho, USA, Idaho Geological Survey Geologic Map 48, https://www.idahogeology.org/product/GM-48 (accessed March 2021).

Kauffman, J.D., Schmidt, K.L., Lewis, R.S., Stewart, D.E., Othberg, K.L., and Garwood, D.L., 2014, Geologic Map of the Idaho Part of the Grangeville 30 x 60 Minute Quadrangle, and Adjoining Areas of Washington and Oregon: Moscow, Idaho, USA, Idaho Geological Survey Geologic Map 50, https://www.idahogeology.org/product/GM-50 (accessed July 2021).

Kirby, E., and Whipple, K., 2001, Quantifying differential rock-uplift rates via stream profile analysis: Geology, v. 29, p. 415–418, https://doi.org/10.1130/0091-7613(2001)029<0415:QDRURV>2.0.CO;2.

Kirchner, J.W., Finkel, R.C., Riebe, C.S., Granger, D.E., Clayton, J.L., King, J.G., and Megahan, W.F., 2001, Mountain erosion over 10 yr, 10 k.y., and 10 m.y. time scales: Geology, v. 29, p. 591–594, https://doi.org/10.1130/0091-7613(2001)029<0591:MEOYKY>2.0.CO;2.

Kohl, C., and Nishiizumi, K., 1992, Chemical isolation of quartz for measurement of in-situ-produced cosmogenic nuclides: Geochimica et Cosmochimica Acta, v. 56, p. 3583–3587, https://doi.org/10.1016/0016-7037(92)90401-4.

Lague, D., 2014, The stream power river incision model: Evidence, theory and beyond: Earth Surface Processes and Landforms, v. 39, p. 38–61, https://doi.org/10.1002/esp.3462.

Lague, D., Hovius, N., and Davy, P., 2005, Discharge, discharge variability, and the bedrock channel profile: Journal of Geophysical Research: Earth Surface, v. 110, F4, https://doi.org/10.1029/2004JF000259.

Lal, D., 1991, Cosmic ray labeling of erosion surfaces: In situ nuclide production rates and erosion models: Earth and Planetary Science Letters, v. 104, p. 424–439, https://doi.org/10.1016/0012-821X(91)90220-C.

Larimer, J.E., Yanites, B.J., Phillips, W., and Mittelstaedt, E., 2019, Late Miocene rejuvenation of central Idaho landscape evolution: A case for surface processes driven by plume-lithosphere interaction: Lithosphere, v. 11, no. 1 p. 59-72, https://doi.org/10.1130/L746.1.

Lewis, R.S., Bush, J.H., Burmester, R.F., Kauffman, J.D., Garwood, D.L., Myers, P.E., and Othberg, K.L., 2005, Geologic Map of the Potlatch 30 x 60 Minute Quadrangle, Idaho: Moscow, Idaho, USA, Idaho Geological Survey Geologic Map 41, https://www.idahogeology.org/product/GM-41 (accessed March 2021).

Lewis, R.S., Burmester, R.F., Kauffman, J.D., Breckenridge, R.M., Schmidt, K.L., McFaddan, M.D., and Myers, P.E., 2007, Geologic Map of the Kooskia 30 x 60 Minute Quadrangle, Idaho: Moscow, Idaho, USA, Idaho Geological Survey Geologic Map 93, https://www.idahogeology.org/product/DWM-93 (accessed March 2021).

Lewis, R.S., Link, P.K., Stanford, L.R., and Long, S.P., 2012, Geologic Map of Idaho: Moscow, Idaho, USA, Idaho Geological Survey.

Lindgren, W., 1904, A geological reconnaissance across the Bitterroot Range and Clearwater Mountains in Montana and Idaho: U.S. Geological Survey Professional Paper 27, 122 p., https://doi.org/10.3133/pp27.

Lindgren, W., and Livingston, D.C., 1918, The Idaho Peneplain: Economic Geology, v. 13, p. 486–492, https://doi.org/10.2113/gsecongeo.13.6.486.

Link, P.K., and Janecke, S.U., 1999, Geology of east-central Idaho: Geologic roadlogs for the Big and Little Lost River, Lemhi, and Salmon River valleys, *in* Hughes, S.S., and Thackray, G.D., eds., Guidebook to the Geology of Eastern Idaho: Pocatello, Idaho, USA, Idaho Museum of Natural History, p. 295–334.

Link, P.K., Crosby, B.T., Lifton, Z.M., Eversole, E.A., and Rittenour, T.M., 2014, The late Pleistocene (17 ka) Soldier Bar landslide and Big Creek Lake, Frank Church-River of No Return Wilderness, central Idaho, U.S.A.: Rocky Mountain Geology, v. 49, p. 17–31, https://doi.org/10.2113/gsrocky.49.1.17.

Lund, K., Snee, L.W., and Evans, K.V., 1986, Age and genesis of precious metals deposits, Buffalo Hump District, central Idaho; implications for depth of emplacement of quartz veins: Economic Geology, v. 81, p. 990–996, https://doi.org/10.2113/gsecongeo.81.4.990.

McQuarrie, N., and Rodgers, D.W., 1998, Subsidence of a volcanic basin by flexure and lower crustal flow: The eastern Snake River Plain, Idaho: Tectonics, v. 17, p. 203–220, https://doi.org/10.1029/97TC03762.

Meyer, G.A., and Leidecker, M.E., 1999, Fluvial terraces along the Middle Fork Salmon River, Idaho, and their

relation to glaciation, landslide dams, and incision rates: A preliminary analysis and river-mile guide, *in* Hughes, S.S., and Thackray, G.D., Guidebook to the Geology of Eastern Idaho: Pocatello, Idaho, USA, Idaho Museum of Natural History, p. 219–235.

Mitchell, N.A., and Yanites, B.J., 2019, Spatially variable increase in rock uplift in the northern U.S. Cordillera recorded in the distribution of river knickpoints and incision depths: Journal of Geophysical Research: Earth Surface, v. 124, p. 1238–1260, https://doi.org/10.1029/2018JF004880.

Montgomery, D.R., and Foufoula-Georgiou, E., 1993, Channel network source representation using digital elevation models: Water Resources Research, v. 29, p. 3925–3934, https://doi.org/10.1029/93WR02463.

Mudd, S.M., Harel, M.-A., Hurst, M.D., Grieve, S.W.D., and Marrero, S.M., 2016, The CAIRN method: Automated, reproducible calculation of catchment-averaged denudation rates from cosmogenic nuclide concentrations: Earth Surface Dynamics, v. 4, p. 655–674, https://doi.org/10.5194/esurf-4-655-2016.

Murphy, B.P., Johnson, J.P.L., Gasparini, N.M., and Sklar, L.S., 2016, Chemical weathering as a mechanism for the climatic control of bedrock river incision: Nature, v. 532, p. 223–227, https://doi.org/10.1038/nature17449.

Niemann, J.D., Gasparini, N.M., Tucker, G.E., and Bras, R.L., 2001, A quantitative evaluation of Playfair's law and its use in testing long-term stream erosion models: Earth Surface Processes and Landforms, v. 26, p. 1317–1332, https://doi.org/10.1002/esp.272.

Parsons, T., Thompson, G.A., and Sleep, N.H., 1994, Mantle plume influence on the Neogene uplift and extension of the US western Cordillera?: Geology, v. 22, p. 83–86, https://doi.org/10.1130/0091-7613(1994)022<0083:MPIOTN>2.3.CO;2.

Pavano, F., Pazzaglia, F.J., and Catalano, S., 2016, Knickpoints as geomorphic markers of active tectonics: A case study from northeastern Sicily (southern Italy): Lithosphere, v. 8, p. 633–648, https://doi.org/10.1130/L577.1.

Perron, J.T., and Royden, L., 2013, An integral approach to bedrock river profile analysis: Earth Surface Processes and Landforms, v. 38, p. 570–576, https://doi.org/10.1002/esp.3302.

Perry-Houts, J., and Humphreys, E., 2018, Eclogite-driven subsidence of the Columbia Basin (Washington State, USA) caused by deposition of Columbia River Basalt: Geology, v. 46, p. 651–654, https://doi.org/10.1130/G40328.1.

Pierce, K.L., and Morgan, L.A., 1992, The track of the Yellowstone hot spot: Volcanism, faulting, and uplift, *in* Link, P.K., Kuntz, M.A., and Piatt, L.B., eds., Regional Geology of Eastern Idaho and Western Wyoming: Geological Society of America Memoir 179, p. 1–54, https://doi.org/10.1130/MEM179-p1.

Pierce, K.L., and Morgan, L.A., 2009, Is the track of the Yellowstone hotspot driven by a deep mantle plume?: Review of volcanism, faulting, and uplift in light of new data: Journal of Volcanology and Geothermal Research, v. 188, p. 1–25, https://doi.org/10.1016/j.jvolgeores.2009.07.009.

Quye-Sawyer, J., Whittaker, A.C., and Roberts, G.G., 2020, Calibrating fluvial erosion laws and quantifying river response to faulting in Sardinia, Italy: Geomorphology, v. 370, https://doi.org/10.1016/j.geomorph.2020.107388.

Reidel, S.P., and Tolan, T.L., 2013, The late Cenozoic evolution of the Columbia River system in the Columbia River flood basalt province, *in* Reidel, S.P., Camp, V.E., Ross, M.E., Wolff, J.A., Martin, B.S., Tolan, T.L., and Wells, R.E., eds., The Columbia River Flood Basalt Province: Geological Society of America Special Paper 497, https://doi.org/10.1130/2013.2497(08).

Reidel, S.P., Fecht, K.R., Hagood, M.C., and Tolan, T.L., 1989, The geologic evolution of the central Columbia Plateau, *in* Reidel, S.P., and Hooper, P.R., eds., Volcanism and Tectonism in the Columbia River Flood-Basalt Province: Geological Society of America Special Paper 239, p. 247–264, https://doi.org/10.1130/SPE239-p247.

Reidel, S.P., Camp, V.E., Tolan, T.L., and Martin, B.S., 2013, The Columbia River flood basalt province: Stratigraphy, areal extent, volume, and physical volcanology, *in* Reidel, S.P., Camp, V.E., Ross, M.E., Wolff, J.A., Martin, B.S., Tolan, T.L., and Wells, R.E., eds., The Columbia River Flood Basalt Province: Geological Society of America Special Paper 497, p. 1–43, https://doi.org/10.1130/2013.2497(01).

Roda-Boluda, D.C., D'Arcy, M., McDonald, J., and Whittaker, A.C., 2018, Lithological controls on hillslope sediment supply: Insights from landslide activity and grain size distributions: Lithological controls on hillslope sediment supply: Earth Surface Processes and Landforms, v. 43, p. 956–977, https://doi.org/10.1002/esp.4281.

Rosenbloom, N.A., and Anderson, R.S., 1994, Hillslope and channel evolution in a marine terraced landscape, Santa Cruz, California: Journal of Geophysical Research: Solid Earth, v. 99, p. 14,013–14,029, https://doi.org/10.1029/94JB00048.

Rowley, D.B., Forte, A.M., Moucha, R., Mitrovica, J.X., Simmons, N.A., and Grand, S.P., 2013, Dynamic topography change of the eastern United States since 3 million years ago: Science, v. 340, p. 1560–1563, https://doi.org/10.1126/science.1229180.

Royden, L., and Perron, T., 2013, Solutions of the stream power equation and application to the evolution of river longitudinal profiles: Journal of Geophysical Research: Earth Surface, v. 118, p. 497–518, https://doi.org/10.1002/jgrf.20031.

Saleeby, J.B., 1983, Accretionary Tectonics of the North American Cordillera: Annual Review of Earth and Planetary Sciences, v. 11, p. 45–73, https://doi.org/10.1146/annurev.ea.11.050183.000401.

Schmidt, J.L., Zeitler, P.K., Pazzaglia, F.J., Tremblay, M.M., Shuster, D.L., and Fox, M., 2015, Knickpoint evolution on the Yarlung river: Evidence for late Cenozoic uplift of the southeastern Tibetan plateau margin: Earth and Planetary Science Letters, v. 430, p. 448–457, https://doi.org/10.1016/j.epsl.2015.08.041.

Schoenbohm, L.M., and Carrapa, B., 2015, Miocene–Pliocene shortening, extension, and mafic magmatism support small-scale lithospheric foundering in the central Andes, NW Argentina, *in* DeCelles, P.G., Ducea, M.D., Carrapa, B., and Kapp, P.A., eds., Geodynamics of a Cordilleran Orogenic System: The Central Andes of Argentina and Northern Chile: Geological Society of America Memoir 212, https://doi.org/10.1130/2015.1212(09).

Schwanghart, W., and Kuhn, N.J., 2010, TopoToolbox: A set of Matlab functions for topographic analysis: Environmental Modelling & Software, v. 25, p. 770–781, https://doi.org/10.1016/j.envsoft.2009.12.002.

Schwanghart, W., and Scherler, D., 2014, Short communication: TopoToolbox 2: MATLAB-based software for topographic analysis and modeling in Earth surface sciences: Earth Surface Dynamics, v. 2, p. 1–7, https://doi.org/10.5194/esurf-2-1-2014.

Scott, D.N., and Wohl, E.E., 2019, Bedrock fracture influences on geomorphic process and form across process domains and scales: Bedrock Fracture Influences on Geomorphology: Earth Surface Processes and Landforms, v. 44, p. 27–45, https://doi.org/10.1002/esp.4473.

Skipp, B., 1987, Basement thrust sheets in the Clearwater orogenic zone, central Idaho and western Montana: Geology, v. 15, p. 220, https://doi.org/10.1130/0091-7613(1987)15<220:BTSITC>2.0.CO;2.

Sklar, L.S., and Dietrich, W.E., 2001, Sediment and rock strength controls on river incision into bedrock: Geology, v. 29, p. 1087–1090, https://doi.org/10.1130/0091-7613(2001)029<1087:SARSCO>2.0.CO;2.

Sklar, L.S., Riebe, C.S., Marshall, J.A., Genetti, J., Leclere, S., Lukens, C.L., and Merces, V., 2017, The problem of predicting the size distribution of sediment supplied by hillslopes to rivers: Geomorphology, v. 277, p. 31–49, https://doi.org/10.1016/j.geomorph.2016.05.005.

Snee, L.W., Lund, K., Sutter, J.F., Balcer, D.E., and Evans, K.V., 1984, The Salmon River Suture Zone, Western Idaho: U.S. Geological Survey Professional Paper 1438.

Staisch, L.M., O'Connor, J.E., Cannon, C.M., Holm-Denoma, C., Link, P.K., Lasher, J., and Alexander, J.A., 2022, Major reorganization of the Snake River modulated by passage of the Yellowstone Hotspot: Geological Society of America Bulletin, v. 134, p. 1834–1844, https://doi.org/10.1130/B36174.1.

Stephenson, S.N., White, N.J., Carter, A., Seward, D., Ball, P.W., and Klöcking, M., 2021, Cenozoic Dynamic Topography of Madagascar: Geochemistry, Geophysics, Geosystems, v. 22, https://doi.org/10.1029/2020GC009624.

Sweetkind, D.S., and Blackwell, D.D., 1989, Fission-track evidence of the Cenozoic thermal history of the Idaho batholith: Tectonophysics, v. 157, p. 241–250, https://doi.org/10.1016/0040-1951(89)90142-X.

Takahahshi, E., Nakajima, K., and Wright, T.L., 1998, Origin of the Columbia River basalts: Melting model of a heterogeneous plume head: Earth and Planetary Science Letters, v. 162, p. 63–80, https://doi.org/10.1016/S0012-821X(98)00157-5.

Tikoff, B., Kelso, P., Manduca, C., Markley, M.J., and Gillaspy, J., 2001, Lithospheric and crustal reactivation of an ancient plate boundary: The assembly and disassembly of the Salmon River suture zone, Idaho, USA, *in* Holdsworth, R.E., Strachan, R.A., Magloughlin, J.F., and Knipe, R.J., eds., The Nature and Tectonic Significance of Fault Zone Weakening: Geological Society, London, Special Publication 186, p. 213–231, https://doi.org/10.1144/GSL.SP.2001.186.01.13.

Tucker, G.E., and Whipple, K.X., 2002, Topographic outcomes predicted by stream erosion models: Sensitivity analysis and intermodel comparison: Journal of Geophysical Research: Solid Earth, v. 107, https://doi.org/10.1029/2001JB000162.

Umpleby, J.B., 1912, An Old Erosion Surface in Idaho: Its Age and Value as a Datum Plane: The Journal of Geology, v. 20, p. 139–147, https://doi.org/10.1086/621941.

U.S. Geological Survey and Idaho Geological Survey, 2018, Quaternary fault and fold database for the United States: https://www.sciencebase.gov/catalog/item/589097b1e4b072a7ac0cae23 (accessed March 2018).

Vogl, J.J., Min, K., Carmenate, A., Foster, D.A., and Marsellos, A., 2014, Miocene regional hotspot-related uplift, exhumation, and extension north of the Snake River Plain: Evidence from apatite (U-Th)/He thermochronology: Lithosphere, v. 6, p. 108–123, https://doi.org/10.1130/L308.1.

von Blanckenburg, F., 2005, The control mechanisms of erosion and weathering at basin scale from cosmogenic nuclides in river sediment: Earth and Planetary Science Letters, v. 237, p. 462–479, https://doi.org/10.1016/j.epsl.2005.06.030.

Wang, Y., Zhang, H., Zheng, D., Yu, J., Pang, J., and Ma, Y., 2017, Coupling slope-area analysis, integral approach and statistic tests to steady-state bedrock river profile analysis: Earth Surface Dynamics v. 5, p. 145–160, https://doi.org/10.5194/esurf-5-145-2017.

Wegmann, K.W., Zurek, B.D., Regalla, C.A., Bilardeool, D., Wollenberg, J.L., Kopczunski, S.E., Ziemann, J.M., Haight, S.L., Apgar, J.D., Zhao, C., and Pazzaglia, F.J., 2007, Position of the Snake River watershed divide as an indicator of geodynamic processes in the greater Yellowstone region, western North America: Geosphere, v. 3, p. 272–281, https://doi.org/10.1130/GES00083.1.

Whipple, K.X., 2004, Bedrock rivers and the geomorphology of active orogens: Annual Review of Earth and Planetary Sciences, v. 32, p. 151–185, https://doi.org/10.1146/annurev.earth.32.101802.120356.

Whipple, K.X., and Tucker, G.E., 1999, Dynamics of the stream-power river incision model: Implications for height limits of mountain ranges, landscape response timescales, and research needs: Journal of Geophysical Research: Solid Earth, v. 104, p. 17661–17674, https://doi.org/10.1029/1999JB900120.

Whipple, K.X., Hancock, G.S., and Anderson, R.S., 2000a, River incision into bedrock: Mechanics and relative efficacy of plucking, abrasion, and cavitation: Geological Society of America Bulletin, v. 112, p. 490–503, https://doi.org/10.1130/0016-7606(2000)112<490:RIIBMA>2.0.CO;2.

Whipple, K.X., Snyder, N.P., and Dollenmayer, K., 2000b, Rates and processes of bedrock incision by the Upper Ukak River since the 1912 Novarupta ash flow in the Valley of Ten Thousand Smokes, Alaska: Geology, v. 28, p. 835–838, https://doi.org/10.1130/0091-7613(2000)28<835:RAPOBI>2.0.CO;2.

Whipple, K.X., DiBiase, R.A., Ouimet, W.B., and Forte, A.M., 2017, Preservation or piracy: Diagnosing low-relief, high-elevation surface formation mechanisms: Geology, v. 45, p. 91–94, https://doi.org/10.1130/G38490.1.

Whittaker, A.C., 2012, How do landscapes record tectonics and climate?: Lithosphere, v. 4, p. 160–164, https://doi.org/10.1130/RF.L003.1.

Willenbring, J.K., Gasparini, N.M., Crosby, B.T., and Brocard, G., 2013, What does a mean mean?: The temporal evolution of detrital cosmogenic denudation rates in a transient landscape: Geology, v. 41, p. 1215–1218, https://doi.org/10.1130/G34746.1.

Willett, S.D., 1999, Orogeny and orography: The effect of erosion on the structure of mountain belts: Journal of Geophysical Research: Solid Earth, v. 104, p. 28,957–28,981, https://doi.org/10.1029/1999JB900248.

Wobus, C., Whipple, K.X., Kirby, E., Snyder, N., Johnson, J., Spyropolou, K., Crosby, B., and Sheehan, D., 2006, Tectonics from topography: Procedures, promise, and pitfalls, *in* Willett, S.D., Hovius, N., Brandon, M.T., and Fisher, D.M., eds., Tectonics, Climate, and Landscape Evolution: Geological Society of America Special Paper 398, p. 55–74, https://doi.org/10.1130/2006.2398(04).

Wood, S.H., 1994, Seismic expression and geological significance of a lacustrine delta in Neogene deposits of the western Snake River plain, Idaho: AAPG Bulletin, v. 78, p. 102–121.

Wood, S.H., and Clemens, D.M., 2002, Geologic and tectonic history of the western Snake River Plain, Idaho and Oregon: Tectonic and Magmatic Evolution of the Snake River Plain Volcanic Province: Idaho Geological Survey Bulletin, v. 30, p. 69–103.

Yang, R., Willett, S.D., and Goren, L., 2015, In situ low-relief landscape formation as a result of river network disruption: Nature, v. 520, p. 526–529, https://doi.org/10.1038/nature14354.

Yuan, H., Dueker, K., and Stachnik, J., 2010, Crustal structure and thickness along the Yellowstone hot spot track: Evidence for lower crustal outflow from beneath the eastern Snake River Plain: Geochemistry, Geophysics, Geosystems, v. 11, n. 3, p. n/a, https://doi.org/10.1029/2009GC002787.

Zhou, Y., 2018, Anomalous mantle transition zone beneath the Yellowstone hotspot track: Nature Geoscience, v. 11, p. 449–453, https://doi.org/10.1038/s41561-018-0126-4.

Zondervan, J.R., Stokes, M., Boulton, S.J., Telfer, M.W., and Mather, A.E., 2020, Rock strength and structural controls on fluvial erodibility: Implications for drainage divide mobility in a collisional mountain belt: Earth and Planetary Science Letters, v. 538, https://doi.org/10.1016/j.epsl.2020.116221.

Science Editor: Mihai Ducea
Associate Editor: Alexander Whittaker

Manuscript Received 22 March 2022
Revised Manuscript Received 9 October 2022
Manuscript Accepted 26 November 2022

Printed in the USA